J. Fluid Mech. (1980), *vol.* 101, *part* 3, *pp.* 449–491
Printed in Great Britain

Vortex pairing in a circular jet under controlled excitation. Part 1. General jet response

By K. B. M. Q. ZAMAN AND A. K. M. F. HUSSAIN
Department of Mechanical Engineering, University of Houston, Texas 77004

(Received 3 January 1979 and in revised form 20 February 1980)

Hot-wire and flow-visualization studies have been carried out in three air jets subjected to pure-tone acoustic excitation, and the instability, vortex roll-up and transition as well as jet response to the controlled excitation have been investigated. The centre-line fluctuation intensity can be enhanced by inducing stable vortex pairing to a level much higher than even that at the 'preferred mode', but can also be suppressed below the unexcited level under certain conditions of excitation. The conditions most favourable to vortex pairing were determined as a function of the excitation Strouhal number, the Reynolds number (Re_D), and the initial shear-layer state, i.e. laminar or turbulent. It is shown that the rolled-up vortex rings undergo pairing under two distinct conditions of excitation: 'the shear layer mode' when the Strouhal number based on the initial shear-layer momentum thickness (St_θ) is about 0·012, and 'the jet column mode' when the Strouhal number based on the jet diameter (St_D) is about 0·85. The former involves pairing of the near-exit thin vortex rings when the initial boundary layer is laminar, irrespective of the value of St_D. The latter involves pairing of the thick vortex rings at $x/D \cong 1{\cdot}75$, irrespective of St_θ or whether the initial boundary layer is laminar or turbulent. For laminar exit boundary layer, pairing is found to be stable, i.e., occurring regularly in space and time, for $Re_D < 5 \times 10^4$, but becomes intermittent with increasing Re_D or fluctuation intensity in the initial boundary layer.

The trajectories of the vortex centres and their convection velocities during a pairing event have been recorded through phase-locked measurements. In the presence of stable vortex pairing, the time average profiles of fluctuation intensities and Reynolds stress show noticeable deviations from those in the unexcited jet. The vortex pairing phenomenon produce considerably larger excursions of the $\widetilde{uv}(t)$ signal than the time-average Reynolds stress reveals, suggesting that only certain phases of the pairing process may be important in entrainment, and production of Reynolds stress and jet noise.

1. Introduction

Although the occurrence of large-scale coherent structures in all turbulent shear flows has neither been confirmed nor universally accepted, their existence in flows that otherwise display all the characteristics of fully-developed turbulence was convincingly demonstrated by Brown & Roshko (1974) and others (e.g. Winant & Browand 1974). These structures, characterized by coherent vortical (lumps of) fluid,

0022-1120/80/4566-2350 $02.00

have length scales of the order of the shear flow width and are believed to play a dominant role in the entrainment, mixing, and presumably, aerodynamic noise production. This 'new look' in shear flow turbulence (Roshko 1976), contrary to the classical notion of essentially complete chaos and randomness, has engendered an unusually high contemporary interest in the large-scale structures. A clearer knowledge of these structures and their interactions is believed to be crucial to the understanding and modelling of shear flow turbulence (Townsend 1956; Liepmann 1976, private communication; Kovasznay 1978; Saffman 1978).

The large-scale structures, especially in the fully-developed turbulent regions, remain hidden under the superimposed, large-amplitude, random fluctuations. Even in the developing regions, where the energetic structures are comparatively easily identifiable, say with the help of flow visualization and high-speed motion pictures (Clark 1979), conventional statistical measurements do not necessarily reveal them. Since there are significant spatial and temporal 'jitters' in their formation, shape, size, orientation, convection velocity, mutual interaction and breakdown, it is a challenging task to unravel and to characterize these structures experimentally, and to infer their dynamical role.

For a comprehensive survey of the literature on the instability and coherent structures in the near-field of a jet, both with and without controlled excitation, see Zaman (1978). The circular jet flow under controlled excitation has been studied by several investigators including Crow & Champagne (1971), Petersen, Kaplan & Laufer (1974), Chan (1974), Browand & Laufer (1975), Bechert & Pfizenmaier (1975) and Moore (1977). Crow & Champagne (1971) observed the formation of orderly 'vortical puffs' in excited axisymmetric jets even when the 'surface ripples' were destroyed by tripping the initial boundary layer and found that maximum amplification of the centre-line fluctuation intensity, i.e. the preferred mode occurred at $St_D = 0{\cdot}30$. However, the conclusions derived from the study of Crow & Champagne may not be universal (Crighton & Gaster 1976). Vlasov & Ginevskiy (1974) found maximum amplification of the centre-line turbulence intensity in a circular jet under external acoustic excitation at $St_D = 0{\cdot}50$, but a significant reduction below the unexcited value at $St_D = 2{\cdot}75$. Petersen *et al.* (1974) also observed suppression of turbulence intensity under excitation; they suggested that vortex pairing was mainly responsible for jet noise. Amplification of broadband jet noise by small-amplitude excitation was found by Bechert & Pfizenmaier (1975) and Moore (1977). Browand & Laufer (1975) studied the differences in the statistical behaviour between the initial rolled-up vortices and the downstream large-scale structure in a circular jet and conjectured that the large-scale structure farther downstream achieves independence from the initial shear-layer vortices through successive stages of vortex pairing.

The lack of a clear understanding of the vortex pairing phenomenon, despite its speculated important role, provided the motivation for the present study. The only detailed quantitative study of the pairing process known is that of Browand & Wiedman (1976) in a plane free shear layer. The detection technique in an uncontrolled flow is not free from ambiguity, and the use of Taylor hypothesis to convert temporal data to spatial information should produce distortion of the measured vortical structures. Organizing the otherwise randomly occurring pairing process by controlled excitation and then carrying out phase-average field measurements is believed to be a superior approach for studying the pairing phenomenon. This latter approach

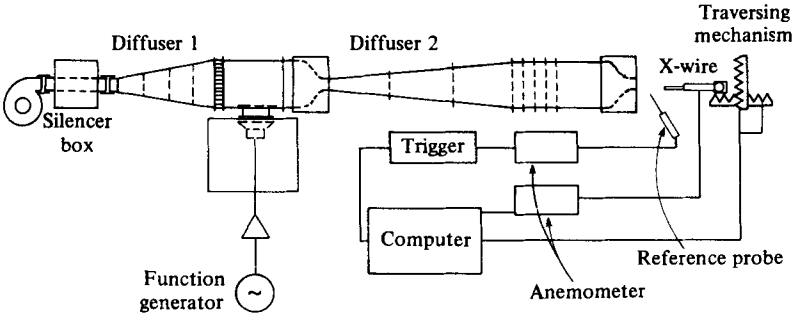

FIGURE 1. Schematic diagram of the flow facility and probe arrangement.

certainly became realistic after the success in the initial phase of this study in 'stabilizing' the pairing process (Hussain & Zaman 1975).

This paper documents the jet response to controlled excitation, and the effects of the Strouhal number, the Reynolds number and initial state on jet instability. The conditions favouring vortex pairing in the circular jet have been explored in detail and the effects of controlled vortex pairing on the jet turbulence structure have been examined. Also included are the convection velocities of the vortices during stable pairing. Part 2 (Hussain & Zaman 1980) explores the analytical and measurement consideration in the study of coherent structure dynamics in general as well as documents the coherent structures and their azimuthal correlations in the jet under conditions of stable vortex pairing.

2. Experimental apparatus and procedures

The experiments were carried out in a circular air jet facility having a 25·4 cm diameter settling chamber and an overall length of 4·7 m (figure 1). The tunnel along with the blower-motor assembly mounted on a separate stand was located at one end of the $15 \times 30 \times 3$ m laboratory with controlled temperature, humidity, and traffic. A six-bladed centrifugal blower coupled to a d.c. motor ($\frac{1}{2}$ h.p.) operated the jet flow facility at controllable speed. The flow from the blower passes through a silencer box, a 10° conical diffuser, a honeycomb, and then into the first settling chamber. It then passes through a 7·62 cm nozzle and a 6° conical diffuser into the second settling chamber (with screens) before exiting through the nozzle. Three nozzles of exit diameters 2·54 cm, 5·27 cm and 7·62 cm used in the study were constructed from laminated wood so that the flow in each case emerged perpendicular to a 30·5 cm end plate. The controllable excitation at the jet exit was introduced by a 25 cm loudspeaker (Jensen, 8 Ω, 50 W) attached to the side of the upstream settling chamber. A perforated curved plate matching the cylindrical contour of the settling chamber was placed in front of the speaker cavity in order to minimize flow disturbance. The loudspeaker, which had a flat response over 100 Hz–2 kHz, was driven by sinusoidal signals from an audio-frequency oscillator via a power amplifier. Most of the experiments were carried out with excitation at one or another of the settling chamber cavity resonance frequencies, although sinusoidal excitation of sufficient amplitude was available at the jet exit at many non-resonant frequencies.

Data were obtained by standard hot-wire techniques employing linearized constant

temperature anemometers (DISA). The experiments were performed under manual control for exploratory studies and under computer control (HP 2100) for automated data acquisition. A spectrum analyser (Spectrascope SD 335) was used to obtain the spectrum $S_u(f)$, defined such that

$$\int_0^\infty S_u^2(f)\,df = \overline{u^2}.$$

Phase measurements were made with the help of a lock-in-amplifier (PAR 129A) and correlations with a correlation function computer (PAR model 101).

3. Results and discussion

3.1. *The flow basic state*

Unless otherwise stated, most data reported in this paper refer to initially untripped boundary layers. Figure 2(*a*) shows the exit boundary-layer mean-velocity U/U_e and longitudinal fluctuation-intensity u'/U_e profiles, measured 0·25 cm upstream from the exit plane. Note the close agreement of the U/U_e data with the Blasius profile. The fluctuation intensity profile with its peak at $(y_w - y)/\delta_e \simeq 1$ is typical of initially laminar jets (Hussain & Clark 1977). The corresponding profiles under excitation at $St_D = 0{\cdot}85$ are also shown in figure 2(*a*). Note that the excitation introduces a sinusoidally oscillating streamwise velocity uniform across the exit plane except for the very thin boundary-layer region. However, the excitation induces no noticeable change in the mean velocity profile in the boundary layer (figure 2*a*) and thus in the exit boundary-layer displacement thickness,

$$\delta_e = \int_0^\infty (1 - U/U_e)\,dy,$$

or the momentum thickness,

$$\theta_e = \int_0^\infty (U/U_e)(1 - U/U_e)\,dy.$$

Within the experimental uncertainty, δ_e/θ_e is found to be close to the Blassius value of 2·59 at all Re_D. The θ_e/D data reasonably well satisfy the relation $\theta_e/D = c_1/\sqrt{Re_D}$ (Becker & Massaro 1968; Browand & Laufer 1975). Values of c_1 were found to be 1·2, 0·79 and 0·52 for jets of diameters 2·54 cm, 5·27 cm and 7·62 cm, respectively. The exit centre-line turbulence intensity u'_{ec}/U_e was found to vary over the range 0·32–0·5 %; an appreciable part of this measured intensity was due to linearizer noise (Zaman 1978).

The exit boundary layers for the 2·54 cm and 7·62 cm jets were considered laminar for the entire available Re_D ranges on the basis of the initial boundary layer mean velocity profiles, shape factors, and fluctuation intensities. For the 5·27 cm jet, the peak turbulence intensity exhibited a sharp rise for $Re_D \gtrsim 70000$ although δ_e and θ_e values above this Re_D agreed with the laminar predictions; the 5·27 cm jet was not used above $Re_D = 70000$. For limited aspects of the study, the boundary layer was tripped with sandpaper rings, 0·4 cm wide and 0·08 cm thick. The trip rings, used only with the 2·54 cm and the 7·62 cm nozzles, were located at 10 cm and 4 cm

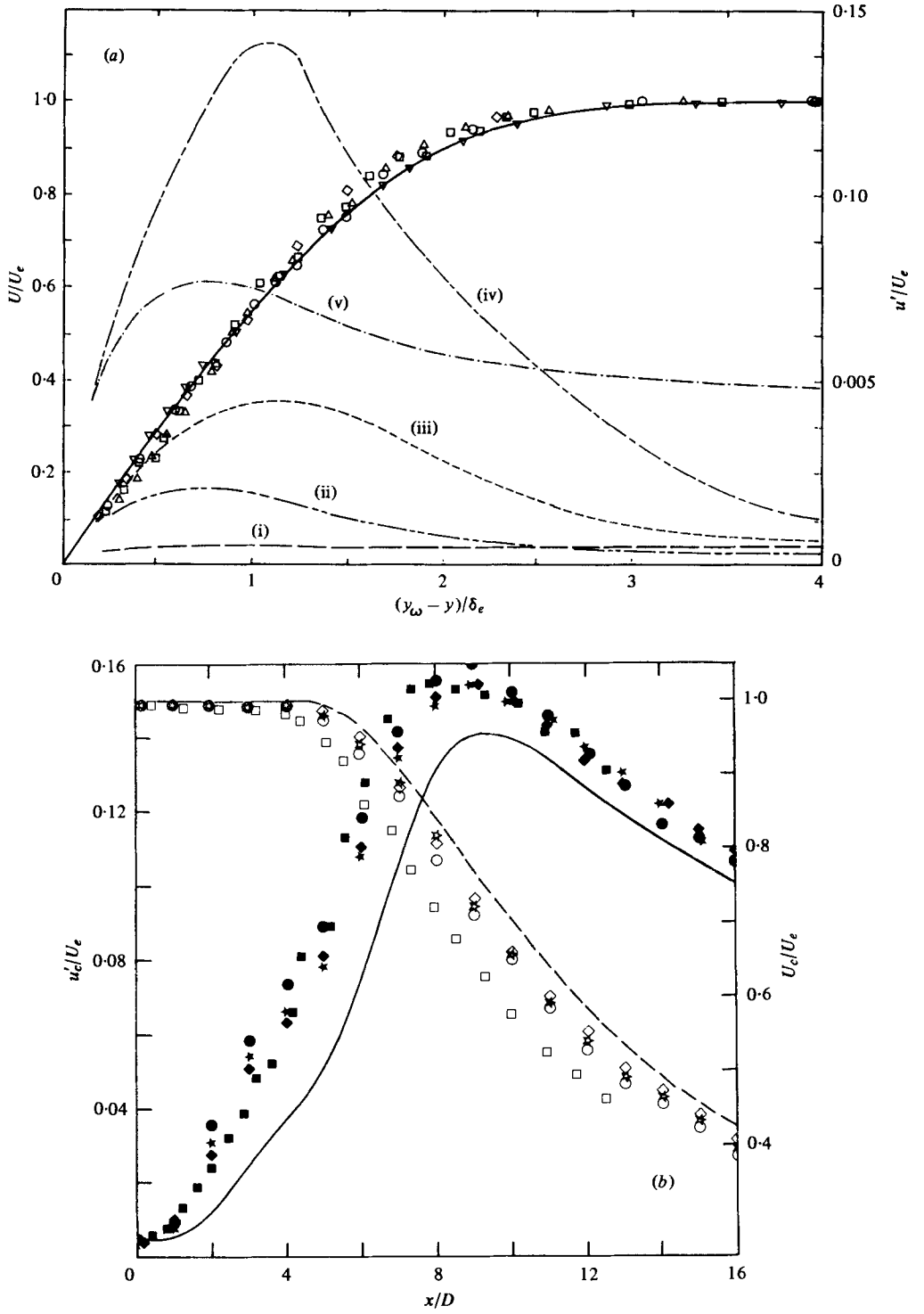

FIGURE 2. (*a*) Exit boundary-layer profiles of U and u'. Jet diameter and Reynolds number are: (i) ▽, 7·62 cm, 32000; (ii) ○, 2·54 cm, 79000; (iii) △, 7·62 cm, 120000; (iv) □, 5·27 cm, 90000; (v) ◇, 7·62 cm (at $St_D = 0{\cdot}85$, $u'_{ec}/U_e = 3\,\%$), 32000. Solid line is the Blasius profile. (*b*) Centre-line variations of u' and U for the 7·62 cm unexcited jet with laminar exit boundary layer at Re_D: □, 32000; ○, 64000; ☆, 92000; ◇, 113000. The lines show Crow & Champagne's (1971) data at $Re_D = 103000$.

upstream from the exit respectively. The logarithmic and wake regions of the mean velocity profiles in (u^+, y^+) co-ordinates, together with the u spectrum and the turbulence intensity profiles in the boundary layer, confirmed that the tripped exit boundary layers were fully turbulent; for further details see Zaman (1978).

Axisymmetry of the near-field jet flow was checked for all of the three nozzles. The $U(y)$ and $u'(y)$ profiles at $x/D = 0{\cdot}25$, 1 and 2 from four radial traverses 90° apart were found to be congruent. The $U(y)/U_e$ profiles as a function of $(y-y_{0{\cdot}5})/\theta$ in the mixing layer were found to be congruent at different x with and without excitation, even though the profiles of fluctuation intensities and Reynolds stress were modified by the excitation.

For the unexcited 7·62 cm jet with laminar exit boundary layer, the centre-line longitudinal mean velocity (U_c) and turbulence intensity (u_c') are shown in figure 2(*b*). The higher decay of U_c at lower Re_D is to be expected (Hill, Jenkins & Gilbert 1975; Hussain & Clark 1977). The mean velocity data at higher Re_D agree fairly with Crow & Champagne's (1971) tripped jet data. There is no clear difference among the $u_c'(x)/U_e$ variations for the four Re_D cases shown, but the data of Crow & Champagne are slightly lower everywhere in x/D.

3.2. *General jet response to controlled excitation*

Figure 3(*a*) shows the downstream (x) variations of the centre-line longitudinal fluctuation intensity u_c'/U_e at different St_D, all for the 2·54 cm jet at the same $Re_D (\cong 12000)$. Note that amplification of u_c' increases with St_D, reaching a maximum at $St_D \simeq 0{\cdot}8$, then decreasing until at $St_D \simeq 1{\cdot}6$ when u_c' values are lower than the corresponding unexcited case. At still higher St_D, the effect of excitation is insignificant. The significant suppression in the near-field centre-line turbulence intensity at $St_D \simeq 1{\cdot}6$, is interesting and pursued separately (Zaman & Hussain 1981). Similar suppression effect was found by Vlasov & Ginevskiy (1974) at $St_D = 2{\cdot}75$, by Rockwell (1972) in the 'preservation regime' excitation of a planar jet, and also by Petersen *et al.* (1974) in a circular jet. Note that the peak of turbulence intensity u_c'/U_e occurs at $x/D \simeq 8$ when the jet is not excited. At some St_D, $u_c'(x)$ develops an earlier peak; this peak increases and shifts upstream as St_D increases. At $St_D \simeq 0{\cdot}8$, the upstream peak is higher than the second peak and is also the highest of all St_D's. As we shall see, this is due to core potential flow fluctuation induced by intense shear layer activity, viz. vortex pairing.

Data similar to those in figure 3(*a*) are shown in figure 3(*b*) for the 7·62 cm jet for $x/D \lesssim 4{\cdot}5$ in order to confirm that the St_D dependence of u_c' is similar to that for the 2·54 cm jet. A possible explanation for the occurrence of the hump at $x/D \simeq 3$ for the unexcited case (figure 3*a*), is that the spatial randomness in vortex roll-up and pairing is reduced at lower Re_D (Clark 1979). Note that at high St_D, there is a dip in u_c'/U_e below its exit value before u_c' starts to grow in x. Transverse profiles of u' at $x/D = 0^+$ and 0·25 showed that this near-exit suppression was uniform across the jet cross-section.

The fundamental r.m.s. amplitude u_f'/U_e on the centre-line is shown in figure 4 for $0 < x/D < 4{\cdot}5$. A few cases around $St_D = 0{\cdot}30$ have been included to emphasize the trend around this St_D. Although the total fluctuation intensity $u_c'(x)$ reaches the highest peak at $St_D \cong 0{\cdot}85$ (figures 3*a*, *b*) maximum growth of u_f' occurs at $St_D = 0{\cdot}30$.

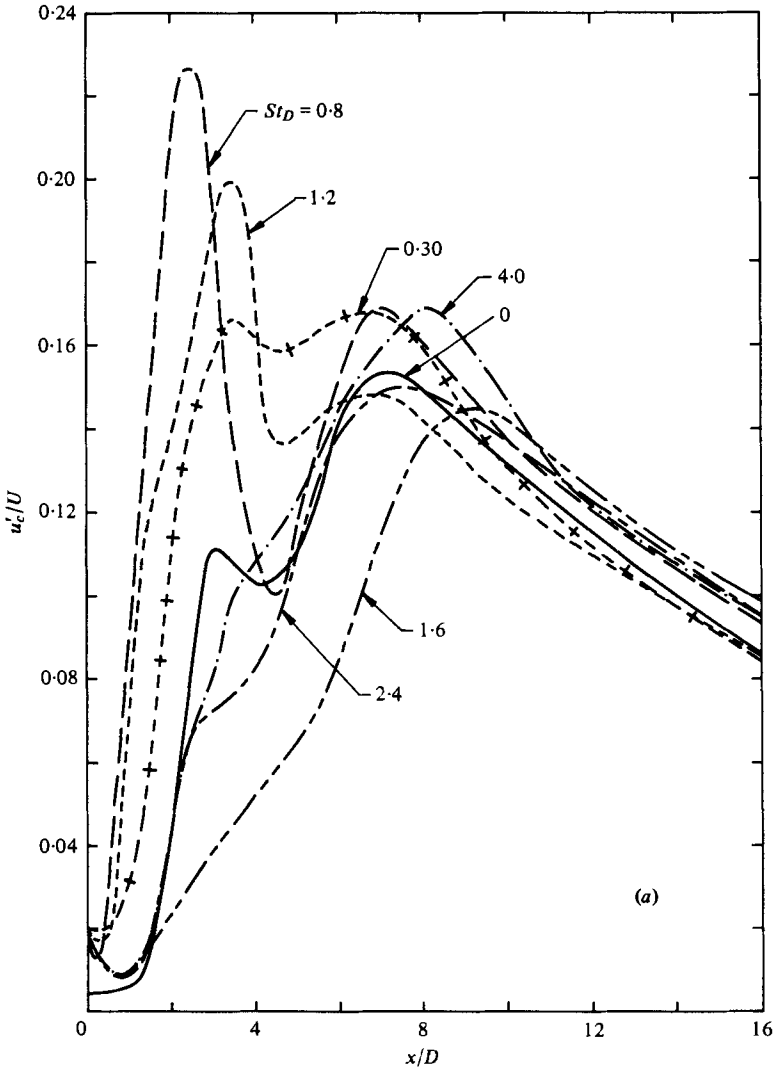

FIGURE 3(*a*). For legend see page 456.

Crow & Champagne (1971) failed to observe the large increase as well as suppression of $u_c'(x)$ presumably because their study was limited to a small St_D range and to jets with tripped boundary layers only. Thus, the Crow and Champagne 'preferred mode' of the round jet should be redefined to be based on u_f' rather than u_c'.

The effect of tripping the initial boundary layer, and thus eliminating the initial shear-layer instability ripples, on the centre-line longitudinal fluctuation intensity variation is shown in figure 5. The conditions at the different St_D's in this figure are the same as in figure 3(*b*) except that the exit boundary layer was turbulent. The $u_c'(x)$ data at $St_D = 0{\cdot}25$, 0·3 and 0·85 do not show the dual-peak variation as they did in figure 3(*a*). The large first peak at $St_D = 0{\cdot}85$ is not present in figure 5(*a*) and only a slight oscillation from a monotonic variation of $u_c'(x)$ can be noticed around $x/D = 2$. This effect of tripping at $St_D = 0{\cdot}85$ will be discussed later. The data at $St_D = 0{\cdot}30$

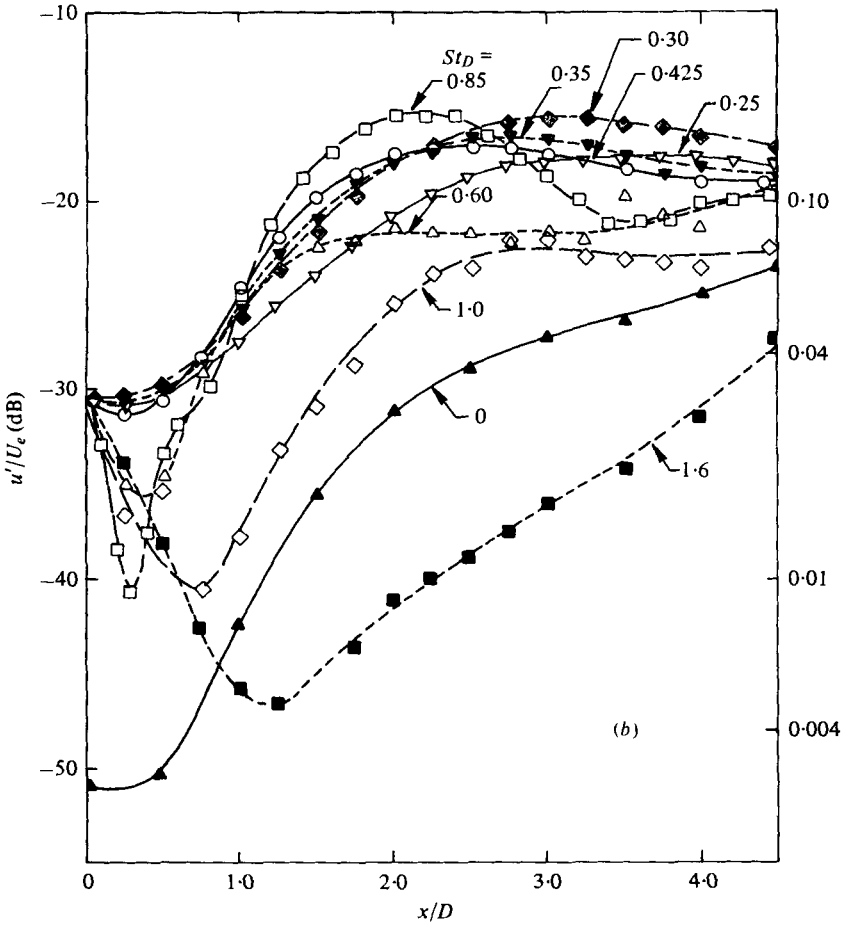

FIGURE 3. (*a*) Dependence of $u_c'(x)$ on St_D for 2·54 cm jet; $Re_D \simeq 12000$. (*b*) St_D dependence of $u_c'(x)$ near the jet exit; $D = 7{\cdot}62$ cm. For $St_D = 0{\cdot}25$, $Re_D = 5{\cdot}0 \times 10^4$; for $St_D = 0{\cdot}85$, $Re_D = 3{\cdot}2 \times 10^4$; for all other St_D's, $Re_D = 4{\cdot}16 \times 10^4$.

still shows large growth of u_c' at $x/D \cong 3$, the value at this location being slightly lower than that for the untripped case. The $u_c'(x)$ variations (figure 5*a*), for example at $St_D = 0{\cdot}30$, is quite different from that shown by Crow & Champagne (1971) which exhibited a sharper and larger first peak. The Reynolds number used by Crow & Champagne ($Re_D = 113000$) for this St_D is much larger than that in the present case (41600). Measurements of $u_c'(x)$ variation at $St_D = 0{\cdot}30$ and at $Re_D = 106000$ (not shown here, see Hussain & Zaman 1975) showed close agreement with Crow & Champagne's data. Thus, the effect of controlled excitation at a St_D on the near-field flow structure must be somewhat dependent on Re_D, even when the latter is large. However, the dependence on St_D is considerably more pronounced. Figure 5(*b*) confirms that $u_f'(x)$ reaches its maximum at $St_D = 0{\cdot}30$, which is the 'preferred mode'.

The circular jet 'preferred mode' thus has been shown to be $St_D = 0{\cdot}30$, irrespective of the exit boundary layer being turbulent or laminar and thus is independent of the exit shear-layer instability characteristics. However, earlier studies with the 2·54 cm

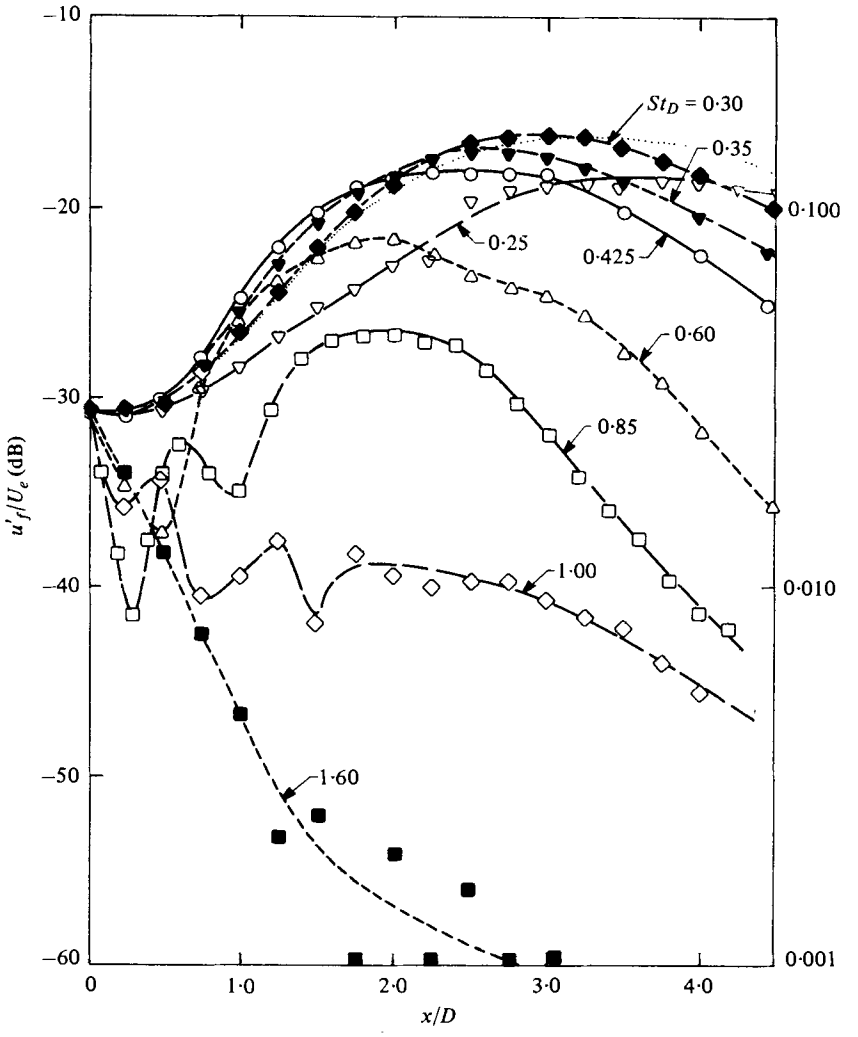

FIGURE 4. Centre-line variation of the fundamental r.m.s. amplitude $u'_f(x)$ for the 7·62 cm jet. Re_D at each St_D are the same as in figure 3 (*b*). ·····, St_D = 0·30, data of Crow & Champagne (1971).

(untripped) jet at still lower Re_D ($\simeq$ 10000) showed that the preferred mode occurred at a somewhat higher St_D ($\simeq$ 0·40). The preferred mode was found to occur at St_D = 0·35 by Chan (1974) and at St_D = 0·50 by Vlasov & Ginevskiy (1974). The variation of the broadband jet noise (due to a small-amplitude excitation) was a maximum at $St_D \cong$ 0·35 in Moore's (1977) experiments. Similar experiments by Bechert & Pfizenmaier (1975) showed a maximum increase in the broadband jet noise at St_D = 0·48. These differences can probably be attributed to differences in the initial condition and the Reynolds number (for example, viscous effects becoming dominant in vortex roll-up at lower Re_D). Crighton & Gaster (1976) have shown that small changes in the mean velocity profile can noticeably alter the axisymmetric shear-layer instability characteristics.

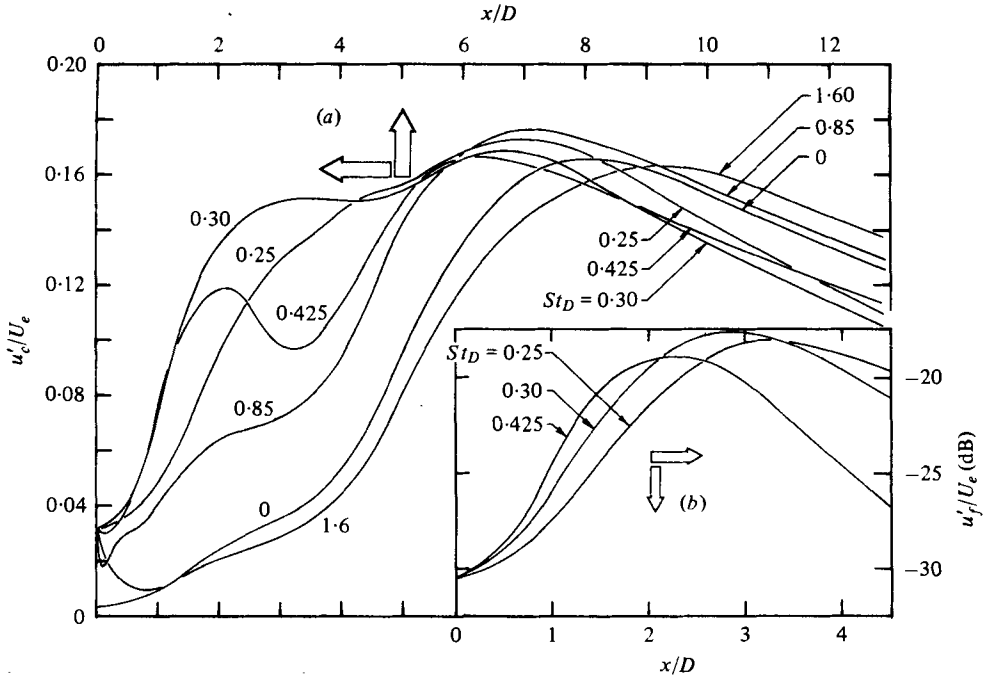

FIGURE 5. (*a*) Dependence of $u_c'(x)$ on St_D in the 7·62 cm jet with tripped exit boundary layer; (*b*) corresponding $u_f'(x)$ data.

3.3. *Stable vortex pairing induced by controlled excitation*

The highest growth rate of $u_c'(x)$ found to occur at $St_D \simeq 0{\cdot}85$ (figure 3), although $u_f'(x)$ exhibited largest growth at $St_D = 0{\cdot}30$ (figure 4), was intriguing and could be explained as follows. The hot-wire signals on the centre-line at $x/D \simeq 2$ and $St_D \simeq 0{\cdot}85$ showed a large-amplitude fluctuation, not at the (fundamental) driving frequency f_p but at its subharmonic $\frac{1}{2}f_p$. The signals showed further that the subharmonic was stable (i.e. periodic in time for any particular location) at comparatively lower Re_D. At higher Re_D, the sub-harmonic formation was characterized by temporal jitter and random occurrence and breakdown.

Oscilloscope traces of the $\tilde{u}$ signal on the centre-line of the 2·54 cm jet at $St_D = 0{\cdot}80$, $Re_D = 8900$ are shown in figure 6. All the traces (*a*)–(*f*) have identical vertical and horizontal scales. As the probe is traversed downstream, the amplitude of the wave first decreases, reaching a minimum at $x/D \cong 0{\cdot}25$ and then starts increasing rapidly. At $x/D \cong 0{\cdot}50$, pairing can be inferred from alternate crests fusing with the next [trace (*b*)]. The formation of an exactly half frequency wave form is complete at $x/D \cong 2$ where the amplitude also reaches its maximum of about 7 times its initial value; the wave form, however, is not sinusoidal [trace (*d*)]. Note the initiation of turbulent breakdown on the centre-line during deceleration following velocity peaks in (*e*). At $x/D = 4$, [trace (*f*)], large random fluctuations mask the still recognizable underlying wave form. But at about $x/D = 6$ (not shown), the signal is totally random without any underlying waveform. Note that until the probe enters the turbulent flow near the end of the potential core, the smooth signal on the centre-line is merely

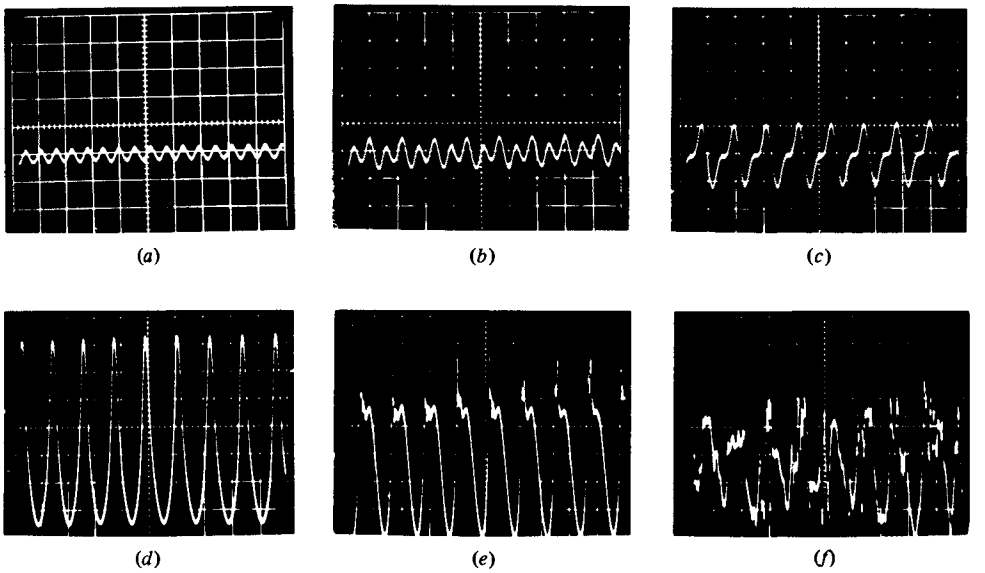

FIGURE 6. Oscilloscope traces of the centre-line $\tilde{u}$ signal in the 2·54 cm jet at different x/D: (*a*) 0; (*b*) 0·5; (*c*) 1·0; (*d*) 2·0; (*e*) 3·0; (*f*) 4·0. $Re_D = 8960$; $St_D = 0{\cdot}80$; $u'_{ec}/U_e = 2\,\%$. The traces are all at the same scale.

the footprint of mixing-layer motions. Thus, only signal near the mixing layer can indicate if the layer is turbulent or not.

Similar frequency-halving of the u signal due to vortex pairing was also observed with the 5·27 and the 7·62 cm jets at $St_D \cong 0{\cdot}85$. (That the subharmonic evolution is directly attributable to vortex pairing is supported by flow-visualization, discussed in § 3.7). The formation of the subharmonic is further explored through measurements of spectra and autocorrelation (figures 7*a*, *b*) of the centre-line $\tilde{u}$ signal at $St_D = 0{\cdot}85$. Note the appearance of the subharmonic component $u'_{\frac{1}{2}f}$ at $x/D = 0{\cdot}5$ from the clean, sinusoidal signal at the exit (figure 7*a*). The subharmonic $u'_{\frac{1}{2}f}$ overtakes the fundamental in amplitude at $x/D \simeq 1$, the region of vortex pairing activity. For $x/D \gtrsim 3{\cdot}5$, energy begins to appear at intermediate frequencies and the spectral peaks become progressively submerged in the evolving, broadband background turbulence. For $x/D \gtrsim 3$, there is a hump at the second subharmonic (i.e. at $\frac{1}{4}f_p$). No successive pairing could be identified from flow visualization. The second subharmonic probably represents initiation of a second pairing which presumably did not materialize due to the limited length before the end of the potential core. The development of higher harmonics does not necessarily suggest the evolution of a smaller-scale structure, but nonlinearity, represented by a non-sinusoidal, distorted signal. True spectral broadening commences at $x/D \simeq 3{\cdot}5$. At $x/D = 6$, the subharmonic peak can hardly be noticed and at $x/D = 8$, it disappears completely. Figure 7 (*b*) essentially duplicates the information content of figure 7 (*a*) since autocorrelation and spectra are Fourier-transform pairs but is included to demonstrate that the autocorrelation sifts out the strongest underlying event (Kibens 1978, private communication).

The Strouhal number dependence of the pairing phenomenon is illustrated in figure 8 through oscilloscope traces of the centre-line $\tilde{u}(t)$ signal for the 5·27 cm jet at $Re_D = 18700$. While in the St_D range 0·7–1·0, the pairing process is repetitive,

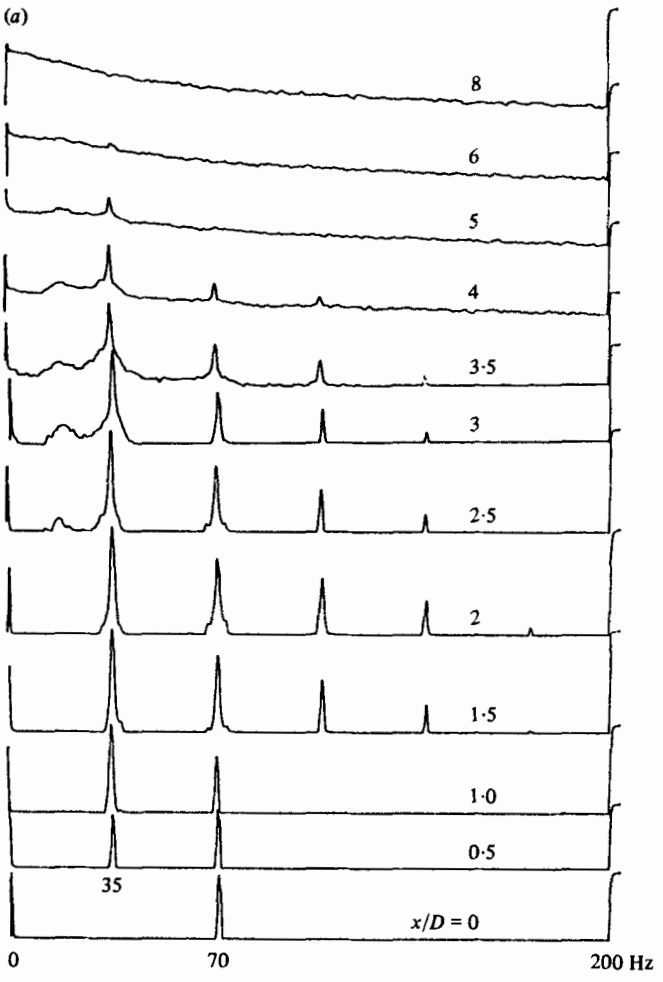

FIGURE 7 (a). For legend see facing page.

pairing is not noticeable at St_D's significantly away from this range. If the value of St_D is close to this range, say $St_D \simeq 1{\cdot}1$, occasional pairing is evident from intermittent formation and breakdown of the half-frequency wave form. The traces for $St_D = 1{\cdot}6$ show that the fluctuation intensities on the centre-line are very low (see figures 3 and 4). At $St_D = 0{\cdot}30$, a higher-harmonic distortion is noticeable at $x/D = 2$ and 2·5, but no subharmonic generation is evident. Traces similar to those in figure 8 for the 2·54 cm and 7·62 cm jets show essentially similar St_D dependence of the pairing phenomenon. The stable vortex pairing phenomenon at $St_D \cong 0{\cdot}85$ was observed in all the three nozzles used in this study for up to $Re_D \cong 50000$. The evolutions of the centre-line hot-wire signal traces (not shown) demonstrate no noticeable dependence on Reynolds number up to $Re_D = 50000$. At higher Re_D, pairing occurred intermittently (discussed later).

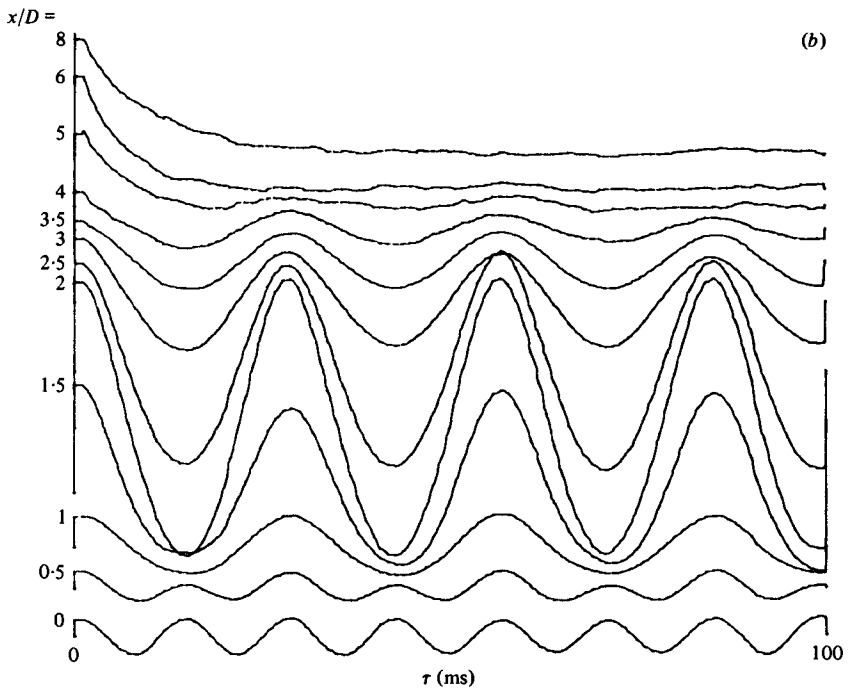

FIGURE 7. (*a*) Spectra and (*b*) autocorrelation of the centre-line $\tilde{u}$ signal for the 7·62 cm jet. $Re_D = 32000$; $St_D = 0{\cdot}85$; $u'_{ec}/U_e = 3\,\%$.

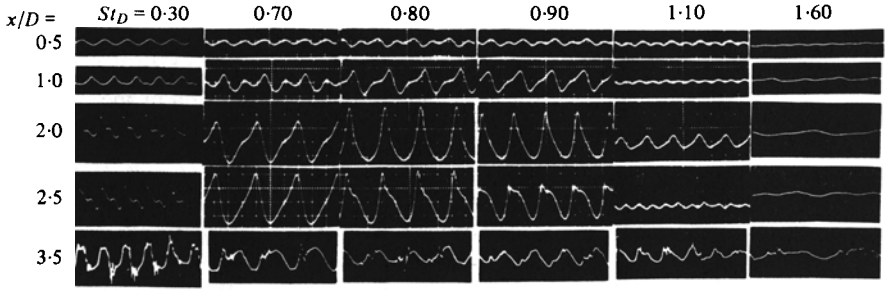

FIGURE 8. Oscilloscope traces of the centre-line $\tilde{u}$ signal at different x and St_D. $D = 5{\cdot}27$ cm; $Re_D = 18700$; $u'_{ec}/U_e = 2\,\%$; the vertical scales are identical but the horizontal scales are arbitrary.

3.4. *The two modes of vortex pairing*

The Reynolds number dependence of the vortex pairing phenomenon at $St_D \cong 0{\cdot}85$ provided motivation for exploring the initial and excitation conditions governing its occurrence. Hot-wire surveys were undertaken to identify on a St_D *vs.* Re_D plot the regions for strong subharmonic formation. It became clear that for a given Re_D, the subharmonic formation also occurred at certain higher St_D's, besides at $St_D \cong 0{\cdot}85$. However, in order to detect the high Strouhal number pairings, the probe had to be moved away from the centre-line, nearer to the shear layer.

Figure 9 shows the spectra of the $\tilde{u}$ signal at indicated off-centre-line probe locations within the potential core, for the cases when vortex pairing can be inferred from the subharmonic peak in the spectra. The probe location was chosen to be $x \simeq 3\lambda$,

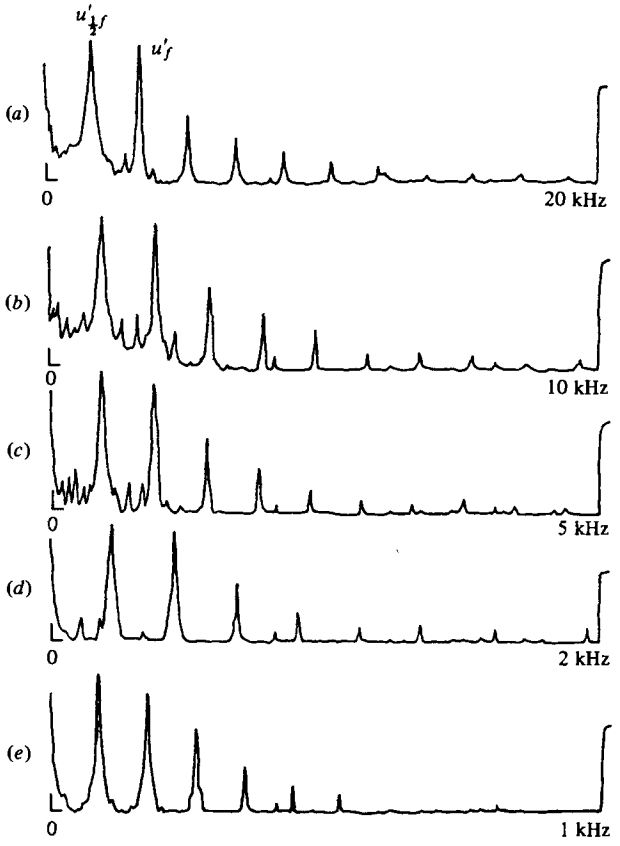

FIGURE 9. Spectra of the $\tilde{u}$ signal for the shear-layer mode of excitation in the 2·54 cm jet. The vertical scales are arbitrary.

	f_p (Hz)	St_D	St_θ	x/D	y/D	u'_{ec}/U_e (dB)
(*a*)	3480	2·65	0·0133	0·61	0·40	−59
(*b*)	1920	2·25	0·0139	0·74	0·38	−57
(*c*)	940	1·61	0·0121	0·94	0·34	−55
(*d*)	452	1·29	0·0125	1·19	0·30	−51
(*e*)	174	0·85	0·0107	1·64	0·23	−47

$y \simeq 0{\cdot}5(D-\lambda)$ after estimating the initial vortex spacing λ on the basis of a convection velocity $v_x \simeq 0{\cdot}5\,U_e$. The small-amplitude excitation levels (u'_{ec}/U_e) were chosen from preliminary surveys which showed that, at the indicated u'_{ec}/U_e levels, the f_p and the $\frac{1}{2}f_p$ spectral components were approximately of equal amplitudes at $x \simeq 2\lambda$ and $y \simeq 0{\cdot}5(D-\lambda)$. The preliminary surveys also indicated that the occurrence of the subharmonic for a given Re_D was dependent only on the Strouhal number and was insensitive to either the exit excitation level or the exact probe location in the flow. Note that the subharmonic amplitude is higher than the fundamental and that the jet Strouhal number St_D ranges from 0·85 to 2·65, while the Strouhal number St_θ based on θ_e is within a small range. Thus, besides occurring at $St_D \cong 0{\cdot}85$ (at any St_θ), strong vortex pairing also occurred when the excitation frequency corresponded to some constant value of St_θ (at any St_D). The value $St_\theta \cong 0{\cdot}012$ was established later to be

the condition favourable for inducing the strongest subharmonic in the latter mode of excitation. This was termed the 'shear-layer mode' of pairing and appears to be the same as the 'matched excitation regime' defined by Rockwell (1972).

For a hyperbolic-tangent mean-velocity profile, Michalke's (1965*a*, *b*) spatial stability-theory prediction for the most unstable disturbance frequency corresponded to $St_\theta = 0{\cdot}0165$. The corresponding value was found experimentally to be 0·017 by Freymuth (1966) in axisymmetric shear layers, 0·018 by Browand (1966) in plane water mixing layer, and 0·017 by Miksad (1972) in a plane air (two-stream) mixing layer. However, the natural roll-up frequency of the exit shear layer in this and other apparatus for our laboratory was found to be at $St_\theta \simeq 0{\cdot}012$, also confirmed by the independent study of the shear layer tone (Hussain & Zaman 1978). Pfizenmaier (1973) also found that the natural roll-up frequency is lower than the most-unstable mode frequency, the latter determined through acoustic excitation. Note that Sato (1960) had found the natural roll-up St_θ in the range 0·009–0·015. This difference between the maximally unstable and the natural roll-up frequencies is being further investigated in our laboratory. Thus, the excitation frequency for the 'shear layer mode' of pairing, i.e. $St_\theta \simeq 0{\cdot}012$, is found to approximately correspond to the natural vortex roll-up frequency of the free shear layer.

Besides in the shear layer mode, stable vortex pairing (i.e. periodic at a certain location) also occurs at the jet Strouhal number $St_D = 0{\cdot}85$ over a large range of Re_D, independent of the value of St_θ. This is termed as the 'jet column mode'. Data establishing the occurrence, as well as characteristics, of the two modes of vortex pairing are discussed below. The non-dimensional characteristic parameters controlling vortex pairing were systematically investigated by hot-wire measurements in the 2·54 cm and 7·62 cm jets, according to the following scheme. For a fixed probe location in the potential core, u spectrum was determined at different U_e, and the fundamental and the subharmonic amplitudes u'_f, $u'_{\frac{1}{2}f}$ were recorded as a function of U_e.

Figure 10(*a*) shows a typical plot of u'_f, $u'_{\frac{1}{2}f}$ variations as functions of U_e (2·54 cm diameter jet); the total turbulence intensity u'_t is also shown for comparison. The sub-harmonic amplitude ($u'_{\frac{1}{2}f}$) peaks at two exit speeds while u'_f variation is smooth; u'_t also shows peaks at the two speeds where $u'_{\frac{1}{2}f}$ has maxima; u'_t at these speeds are essentially due to the subharmonic. Note that above $U_e = 21$ m s^{-1} the subharmonic disappears; the fluctuation intensity is essentially due to the fundamental; and u'_f is much smaller than $u'_{\frac{1}{2}f}$ when $St_\theta \simeq 0{\cdot}012$ ($U_e \simeq 9$ m s^{-1}) or $St_D \simeq 0{\cdot}79$ ($U_e \simeq 14{\cdot}5$ m s^{-1}). The power input to the loudspeaker was kept the same throughout the experiment after setting $u'_e/U_e = 1$ % at 10 m s^{-1}. This resulted in a continuous variation in u'_e/U_e, being higher at lower speeds (as high as 3 %) and lower at higher speeds (as low as 0·5 %). This, however, did not affect the locations of the two peaks. Figure 10(*b*) shows $u'_{\frac{1}{2}f}$ as a function of U_e for the same conditions as in figure 10(*a*) but for three different exit excitation levels u'_e/U_e namely 0·3 %, 1·0 %, and 3·0 % (reset for each data point); the probe location was the same, i.e. at $x/D = 2$ on the centre-line. This figure demonstrates that vortex pairing can be induced for a wide range in the exit excitation amplitude and the two speeds where $u'_{\frac{1}{2}f}$ reach maxima remain essentially unaltered with changing u'_e/U_e.

We briefly digress here to describe the jet response to excitation amplitude u'_{fe} for the jet-column mode of pairing ($St_D = 0{\cdot}85$). The values of u'_t, u'_f and $u'_{\frac{1}{2}f}$ measured at $x/D = 2$ on the centre-line as functions of u'_{fe} are shown in figure 11 for $St_D = 0{\cdot}85$.

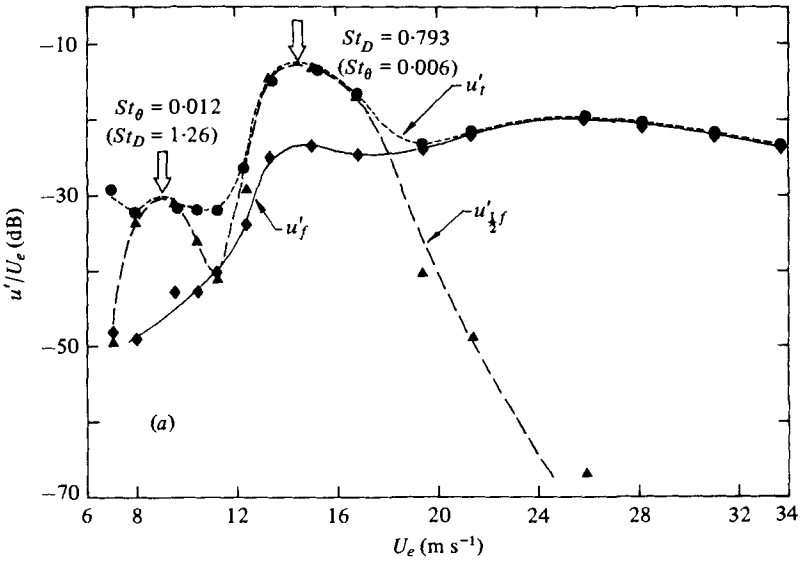

FIGURE 10(*a*). For legend see facing page.

The subharmonic amplitude variation indicates that, at low values of u'_{fe}/U_e (e.g. at -45 dB), pairing is a weak event, but with increasing u'_{fe}, the fundamental amplitude u'_f at first decays while $u'_{\frac{1}{2}f}$ grows, i.e. pairing becomes progressively stabilized. At about $u'_{fe}/U_e = -42$ dB, u'_f starts to increase again; this can be attributed to the beginning of nonlinear saturation of $u'_{\frac{1}{2}f}$ when energy begins to become distributed at higher harmonics of $\frac{1}{2}f_p$, e.g. f_p. At about $u'_{fe}/U_e = -38$ dB (1·3 %), $u'_{\frac{1}{2}f}$ constitutes almost all of u'_t. Note that at $St_D \simeq 0{\cdot}85$, u'_f is much smaller than u'_t. This contrasts with the preferred mode of excitation ($St_D \simeq 0{\cdot}30$) when u'_t is essentially due to u'_f.

Returning to the bimodal nature of vortex pairing, the values of U_e corresponding to the two peaks in figures 10(*a*, *b*) are found to be quite insensitive to the probe location. Figure 12 shows that U_e for the peak subharmonic response detected by a hot-wire at three different physical locations are the same as in figures 10(*a*, *b*). Of course, the $u'_{\frac{1}{2}f}$ varies because it depends on the distance of the probe from the event in question.

Figure 13(*a*) shows data similar to figure 10(*a*) for a distinctly different excitation frequency, namely, 1004 Hz; $u'_{\frac{1}{2}f}$ shows two clear peaks corresponding to $St_\theta \simeq 0{\cdot}011$ and $St_D \simeq 0{\cdot}90$. When St_D is high, the shear layer mode is found to involve more than one stage of pairing; the peak of $u'_{\frac{1}{2}f}$ curve in such a case no longer corresponds to $St_\theta \simeq 0{\cdot}012$. Note that in figure 13(*b*), which is for the 7·62 cm jet at $f_p = 70$ Hz, the $u'_{\frac{1}{4}f}$ spectral component has its peak at the U_e corresponding to $St_\theta \simeq 0{\cdot}012$.

Depending on the axial location of the probe, a particular stage of pairing, say the second (i.e. at $\frac{1}{4}f_p$), may be captured in the velocity signal. Due to a normally encountered non-sinusoidal periodicity (see, for example, in figure 6) the spectrum of this signal will be marked by a predominant $u'_{\frac{1}{4}f}$ component as well as its harmonics, namely, the $u'_{\frac{1}{2}f}$, u'_f components, etc. In this situation, only the $\frac{1}{4}f_p$ value bears a physical significance, being the passage frequency of the vortices after 2 stages of pairing. As we will further show later, the growth of the $u'_{\frac{1}{4}f}$ component with x marks

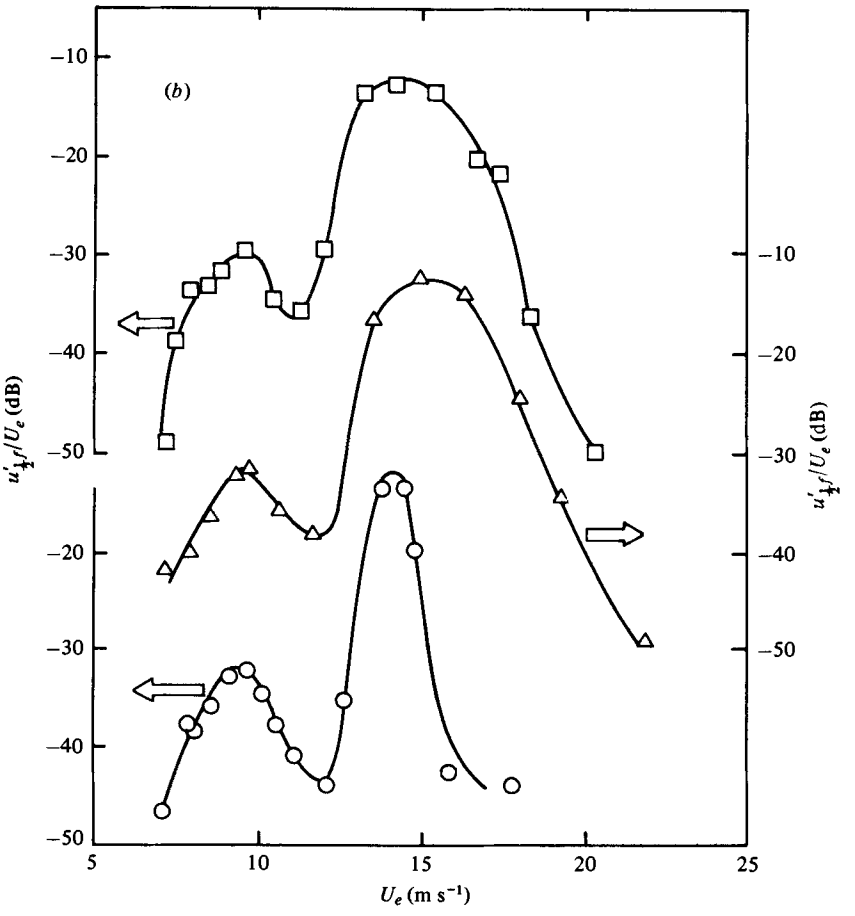

FIGURE 10. (*a*) Variations of the r.m.s. amplitudes u'_t, u'_f and $u'_{\frac{1}{2}f}$ at different U_e in the 2·54 cm jet at $x/D = 2$, $y/D = 0$; $f_p = 452$ Hz; $u'_{ec}/U_e = 1$ % at $U_e = 10$ m s^{-1}. (*b*) Dependence of $u'_{\frac{1}{2}f}$ on U_e in the 2·54 cm jet at excitation levels: ○, $u'_{fe}/U_e = 0{\cdot}3$ %; △, $u'_{fe}/U_e = 1$ %; □, $u'_{fe}/U_e = 3$ %.

the change-over of a waveform at $\frac{1}{2}f_p$ to one at $\frac{1}{4}f_p$, and a corresponding decay in the $u'_{\frac{1}{2}f}$ component. Thus, the peak in the $u'_{\frac{1}{4}f}$ component in figure 13(*b*) represents the condition most conducive to shear layer mode of pairing. If the probe were located farther downstream, the $u'_{\frac{1}{4}f}$ peak value may be higher than the $u'_{\frac{1}{2}f}$ peak value; however, the probe then may also pick up a $u'_{\frac{1}{8}f}$ component from a later pairing event. Thus, while the relative amplitudes of the subharmonics recorded by a sensor depend on its location, the St_θ would represent the pairing event only when it is formed with the U_e corresponding to the peak of the lowest subharmonic amplitude recorded. Note that in the computation of St_θ in figure 13(*b*), the frequency used is still f_p and not $\frac{1}{4}f_p$.

Figure 13(*c*) corresponds to the same conditions as in figure 13(*b*) except that the probe location is farther downstream, namely at $x/D = 2$ (on the centre-line). A third stage shear layer mode of pairing occurs for a small range of U_e, and the peak of $u'_{\frac{1}{8}f}$ component now corresponds to $St_\theta \simeq 0{\cdot}012$ while $u'_{\frac{1}{2}f}$ and $u'_{\frac{1}{4}f}$ components have broad peaks. Figure 13(*d*) shows one more set of similar data for the 7·62 cm jet with $f_p = 110$ Hz. The $u'_{\frac{1}{4}f}$-peak in this figure corresponds to the 'shear layer mode'; the $u'_{\frac{1}{2}f}$ dependence of U_e varies widely but its peak amplitude corresponds to the jet column mode ($St_D = 0{\cdot}85$).

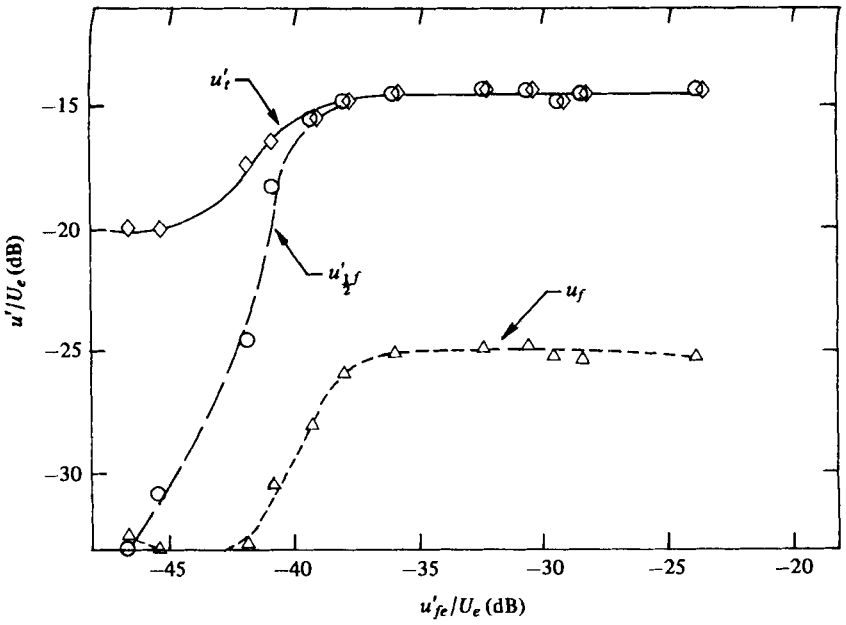

FIGURE 11. Dependence of u'_j, $u'_{\frac{1}{2}f}$ and u'_t on u'_{fe} at $x/D = 2{\cdot}0$ and $y/D = 0$; $D = 7{\cdot}62$ cm; $Re_D = 32000$ and $St_D = 0{\cdot}85$.

In order to further confirm the Strouhal numbers associated with the two modes of vortex pairing, it is desirable to show the jet response for fixed velocities but varying frequencies of excitation. However, the frequencies of excitation as well as excitation amplitudes, being determined by the settling chamber cavity resonance characteristics, cannot be varied continuously. It was possible to obtain such data only for a limited number of cases at relatively lower frequencies (f_p); see figure 13(*e*). Sinusoidal excitation of sufficient amplitude was not available in the dashed range. This figure covers data with two different probe locations. The subharmonic curves are characterized by two peaks: the one on the right representing the shear layer mode and the other, the jet column mode.

The results from figure 10 and 13 and several others (not shown) are summarized in figure 14. The loci of the two modes of vortex pairing are shown here on a St_D *vs.* $Re_D^{\frac{1}{2}}$ plot. For the jet column mode, the vortex pairing is stable for up to $Re_D^{\frac{1}{2}} \cong 220$, while the shear layer mode pairing was found to have irregularities (i.e. jitter) throughout the available Re_D ranges. Both the regions terminate on the left because of difficulty in measurements at low velocities or non-availability of sinusoidal excitations at very low frequencies. A f_p = constant line will intersect the loci for the two modes at two different values of Re_D (figure 14). Note that on a St_θ *vs.* Re_θ plot, while the shear layer mode curves for the two jets would coincide at $St_\theta \simeq 0{\cdot}012$, the jet column mode curves for the two jets would be apart.

3.5. *Characteristics of the two modes of pairing*

In order to understand further the shear-layer mode, the downstream spectral evolution in the shear layer was studied with the hot-wire traversed along the $U/U_e = 0{\cdot}70$

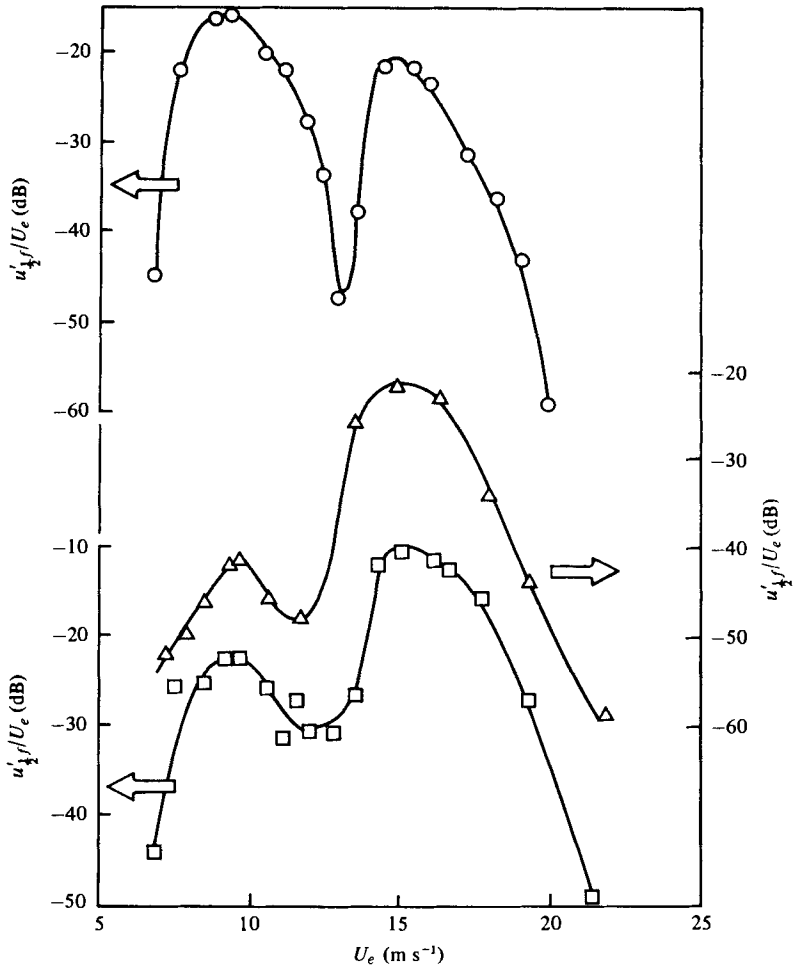

FIGURE 12. Variation of $u'_{\frac{1}{4}f}$ with U_e for three different probe locations: ○, $x/D = 2$, $U/U_e = 0{\cdot}99$; △, $x/D = 2$, $y/D = 0$; □, $x/D = 1$, $U/U_e = 0{\cdot}99$. $D = 2{\cdot}54$ cm; $f_p = 452$ Hz; $u'_{fe}/U_e = 1\,\%$.

line. Figure 15 (*a*) shows the downstream variation of u'_t and other spectral components for the 7·62 cm jet for excitation at $St_\theta = 0{\cdot}011$. Values of U_e and f_p were chosen such that $St_D\,(= 3{\cdot}77)$ was so high that no appreciable part of the signal could be due to the jet-column mode. While the higher-harmonic amplitudes show considerable scatter in the data, possibly due to background noise, the $u'_{\frac{1}{4}f}$, $u'_{\frac{1}{2}f}$ and u'_f spectral components exhibit well defined trends.

The fundamental u'_f, which initially grows exponentially with x, saturates at $x/D \cong 0{\cdot}15$. The saturation and subsequent decay of u'_f is associated with the growth of its harmonics, but more importantly that of the subharmonic. The maximum growth rate of the subharmonic roughly coincides with the location of the saturation of the fundamental; at this location u'_f/U_e is 10 %, which is close to the theoretical value (12 %) predicted by Kelly (1967). The subharmonic grows to an amplitude larger than u'_f (possibly partly because of the addition of kinetic energy of two like-signed vortices) saturates farther downstream at $x/D \simeq 0{\cdot}30$, and then decays. The saturation of the subharmonic generates its own harmonics and thus causes u'_f to

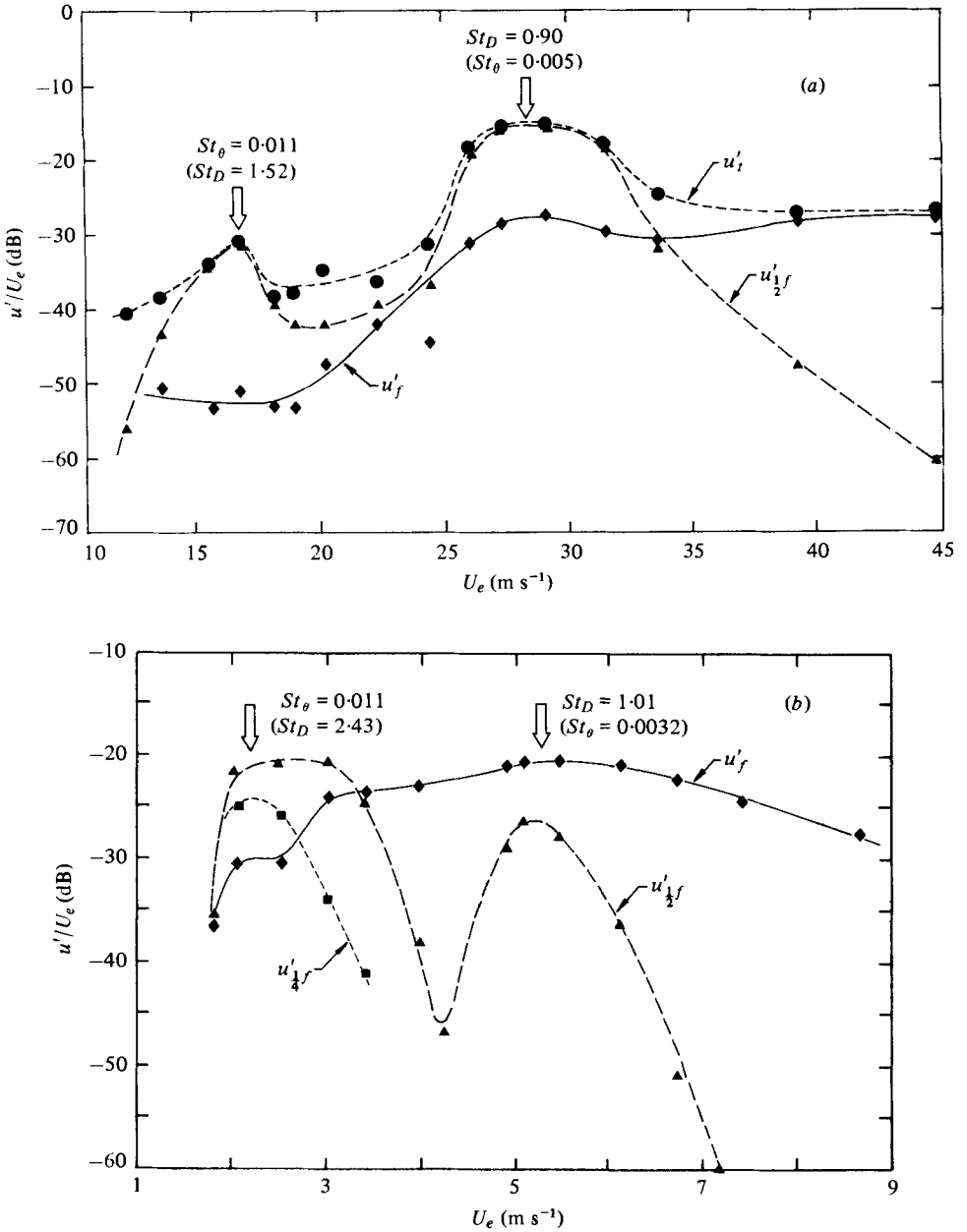

FIGURE 13(*a*, *b*). For legend see page 470.

rise again. A similar sequence of events follows farther downstream with the generation of the second subharmonic, until at $x/\theta_e \simeq 250$, where decay of all the harmonic and subharmonic peaks begin, leading to turbulent breakdown.

The streamwise evolution of the instability modes in the axisymmetric free shear layer shown in figure 15(*a*) may be compared to the plane free shear-layer data of Miksad (1972). For this figure, one may identify eight approximate regions of disturbance growth, marked in the figure. Miksad's (1972) plane shear-layer data show

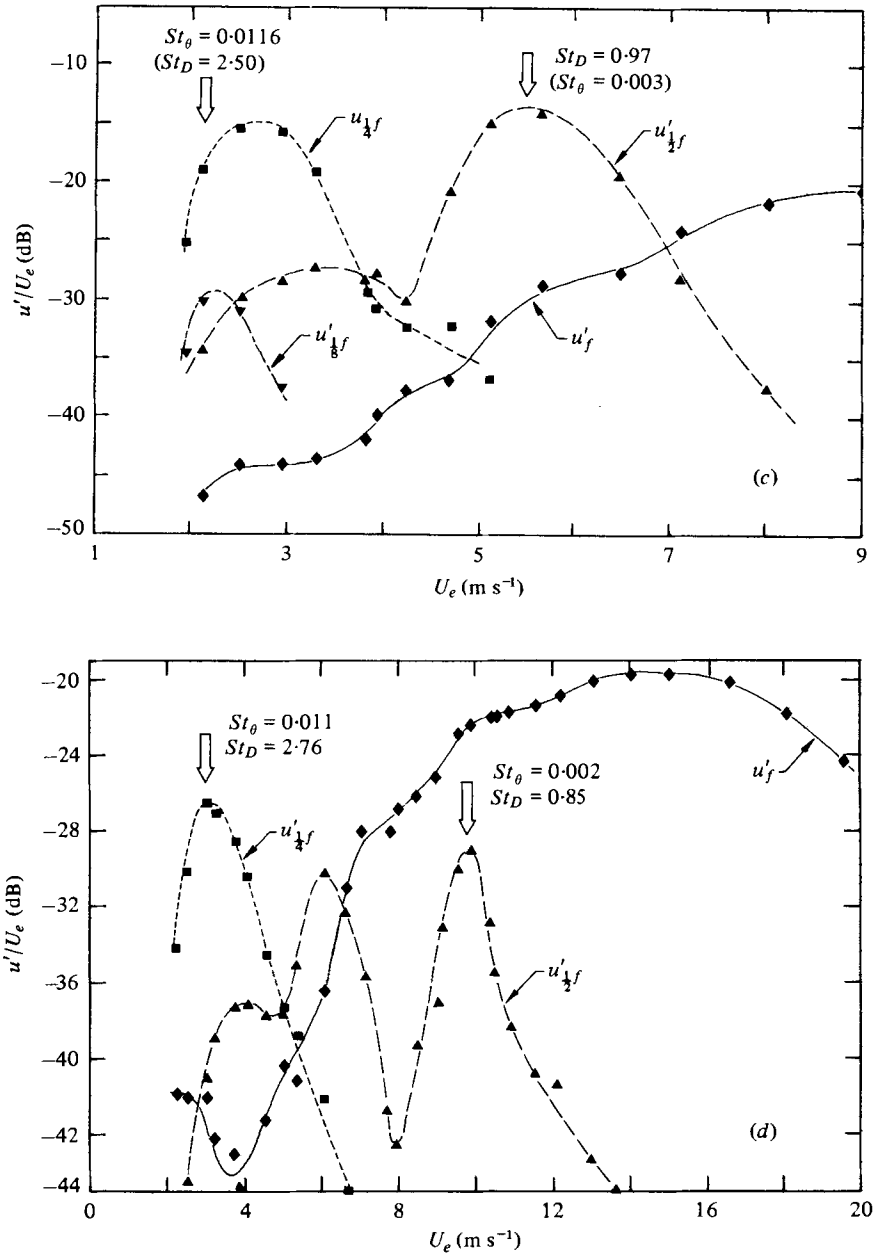

FIGURE 13 (*c*, *d*). For legend see page 470.

peaks much wider in x than ours but show no subsequent peaks in u'_f, $u'_{\frac{1}{2}f}$ beyond the first. Also, while only one stage of pairing is indicated in Miksad's data, our data show at least two successive stages of pairing. The pairing event in the axisymmetric mixing layer which involves leap-frog motions of the ring vortices, is expected to be more intense than in the plane shear layer. It is not clear if the configuration differences between Miksad's experiment and ours can explain the differences in the data. However, while Winant & Browand (1974) have evidenced continued pairings even in the

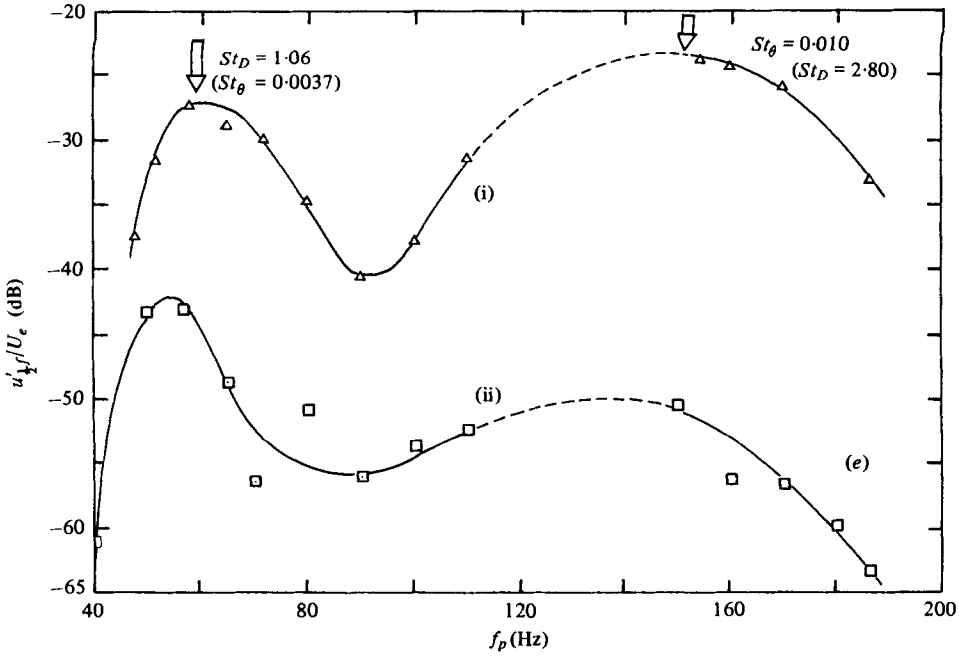

FIGURE 13. (*a*) Variations of u'_f, $u'_{\frac{1}{2}f}$ and u'_t with U_e in the 2·54 cm jet. f_p = 1004 Hz; u'_{ec}/U_e = 1 % at U_e = 19 m s^{-1}; probe at x/D = 2, y/D = 0. (*b*) Variations of u'_f, $u'_{\frac{1}{2}f}$ and $u'_{\frac{1}{4}f}$ with U_e in the 7·62 cm jet. f_p = 70 Hz; u'_{ec}/U_e = 3 % at U_e = 2·4 m s^{-1}; probe at x/D = 0·67, y/D = 0. (*c*) Variations of u'_f, $u'_{\frac{1}{2}f}$, $u'_{\frac{1}{4}f}$ and $u'_{\frac{1}{8}f}$ with U_e. Conditions same as in (*b*) except probe at x/D = 2·0, y/D = 0. (*d*) Variations of u'_f, $u'_{\frac{1}{2}f}$ and $u'_{\frac{1}{4}f}$ with U_e in the 7·62 cm jet. f_p = 110 Hz; u'_{ec}/U_e = 3 % at U_e = 5 m s^{-1}. Probe at x/D = 1·5, y/D = 0·3. (*e*) Variations of $u'_{\frac{1}{2}f}$ amplitude with the excitation frequency f_p in the 7·62 cm jet at U_e = 4·1 m s^{-1}. Probe location: (i) x/D = 0·67, U/U_e = 0·95; (ii) x/D = 0·67, y/D = 0.

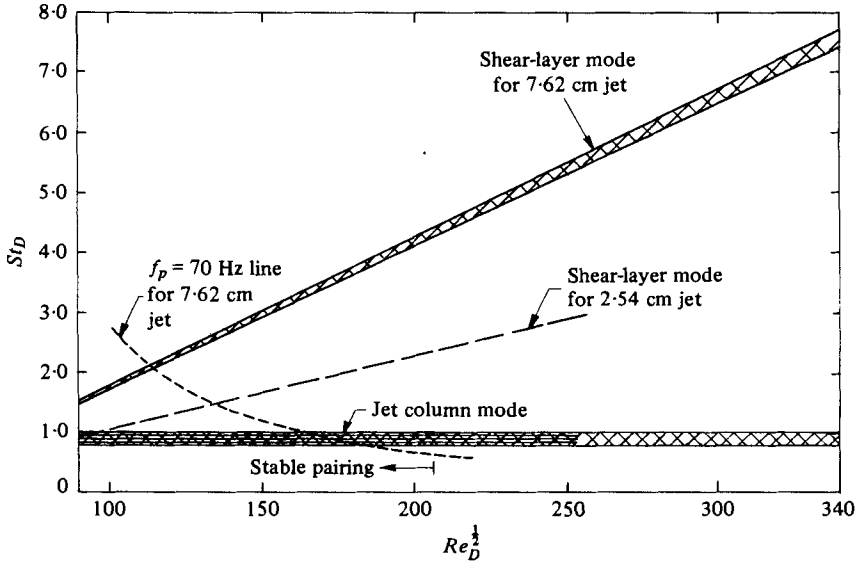

FIGURE 14. Conditions of excitation conducive to vortex pairing.

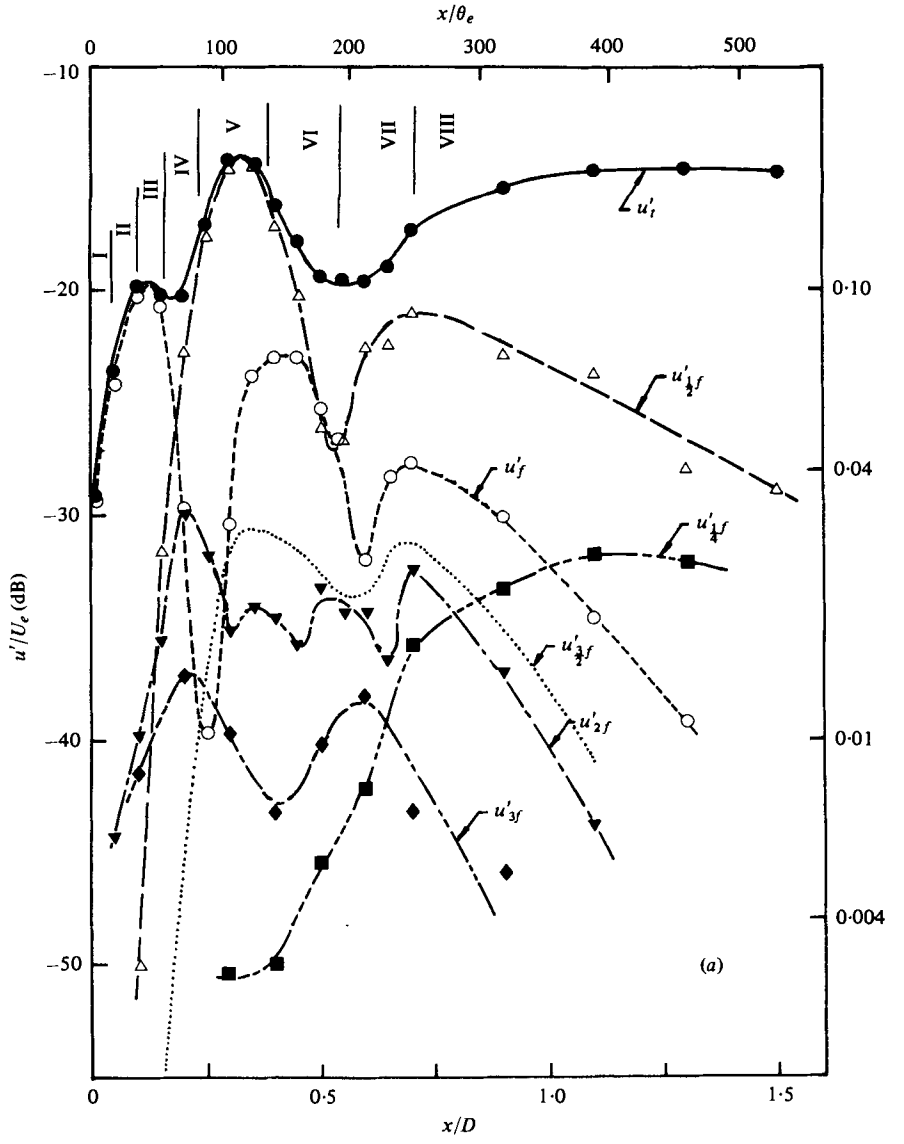

FIGURE 15(*a*). For legend see page 472.

self-preserving turbulent shear layer, it is surprising that Miksad's data suggest only one stage of pairing.

The streamwise evolution of $u'_{\frac{1}{2}f}$ (along the $U/U_e = 0{\cdot}70$ line) is shown in figure 15(*b*) for a few St_θ cases. Below $St_\theta = 0{\cdot}006$, there was no distinct peak (or hump) in the spectra at $\frac{1}{2}f_p$, nor was there any above $St_\theta = 0{\cdot}015$. The initial subharmonic growth is essentially exponential, the growth rate progressively increasing with St_θ until reaching a maximum at $St_\theta \simeq 0{\cdot}011$ and then decreasing at higher St_θ. The peak amplitude of the $St_\theta = 0{\cdot}011$ case also occurs nearest to the exit.

For the jet-column mode, the (centre-line) streamwise spectral evolution is shown

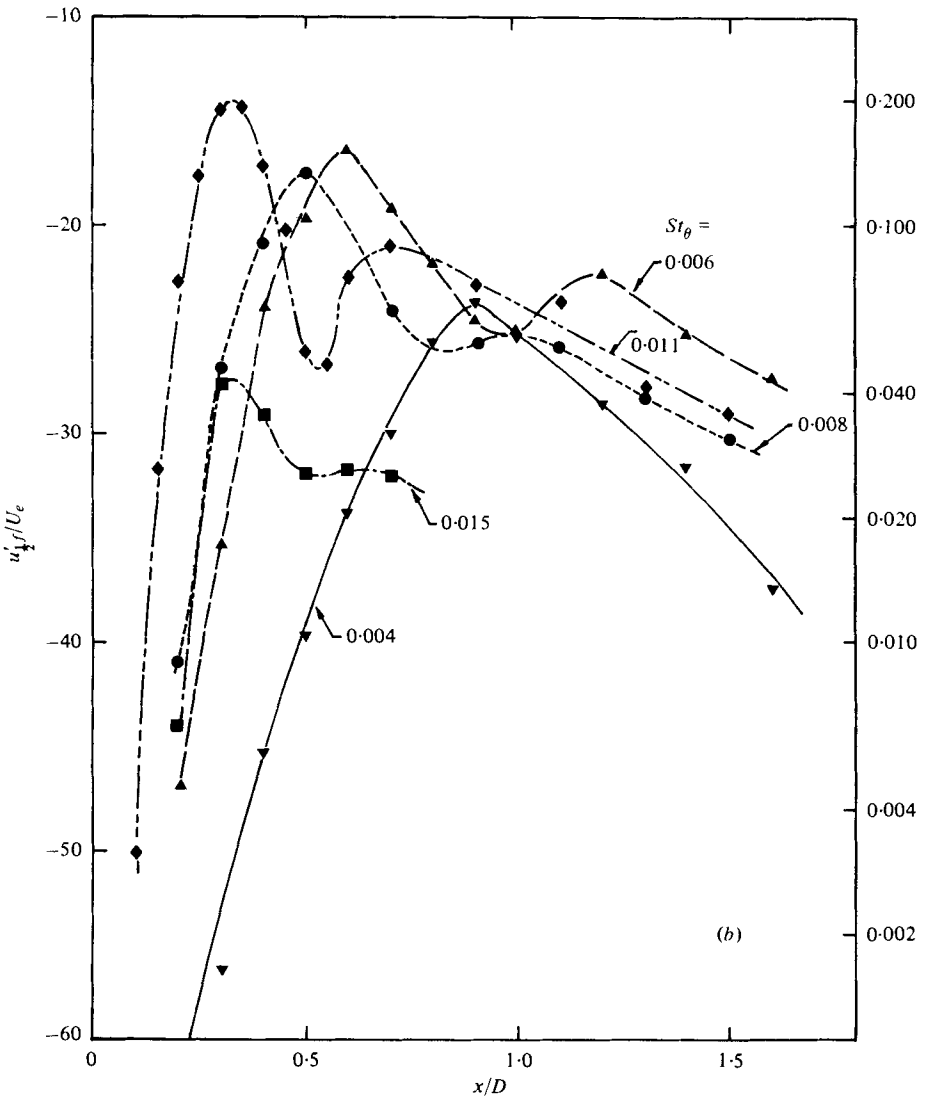

FIGURE 15. (*a*) Evolution of spectral amplitudes in the shear-layer mode $St_\theta = 0{\cdot}011$ ($St_D = 3{\cdot}77$); (*b*) dependence of $u'_{\frac{1}{2}f}(x)$ on St_θ. $D = 7{\cdot}62$ cm; $f_p = 308$ Hz; $u'_{ec}/U_e = 1\,\%$. Traverse along $U/U_e = 0{\cdot}70$ line.

in figure 16(*a*). Immediately downstream from the exit, the signal is due to the fundamental component which first decreases, then grows and saturates due to the growth of the subharmonic through pairing. The pairing event is a relatively violent stage of vortex motion which produces an intensification of the induced velocity oscillations around the vortices. The subharmonic grows and reaches a maximum at $x/D \simeq 2{\cdot}5$ before saturation. In this region, the total signal is essentially due to the subharmonic and the fundamental then rises again due to the saturation of the subharmonic. The discussion here essentially follows that in connexion with figure 15(*a*). Like the different regions of instability of the shear layer, the evolution of the disturbance on the jet centre-line (figure 16*a*) may be identified by seven different stages marked in the figure.

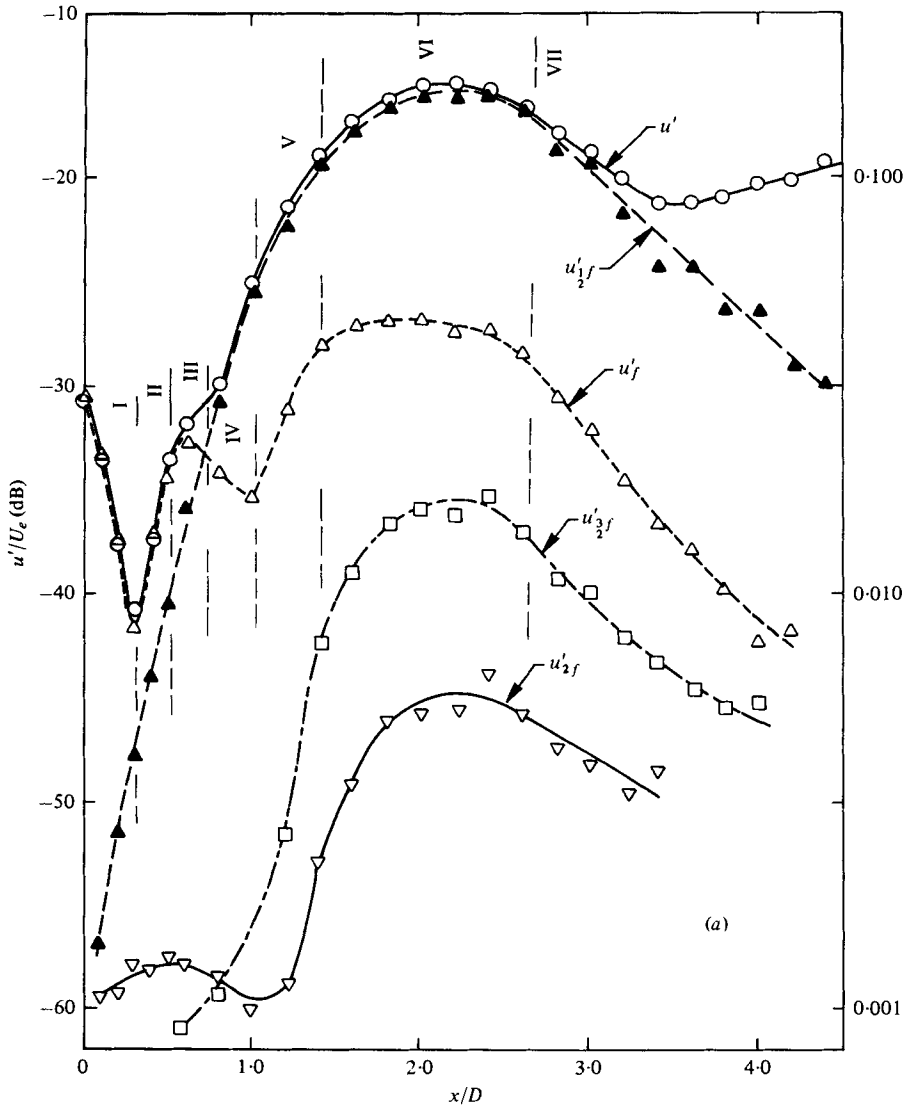

FIGURE 16(*a*). For legend see page 474.

The growth of the subharmonic for the jet-column mode as a function of x/D (on the centre-line) for different St_D is plotted in figure 16(*b*). This figure confirms that the maximum growth rate as well as peak amplitude of the subharmonic occurs at $St_D = 0{\cdot}85$ (for the jet column mode). The subharmonic formation did not occur for cases below $St_D = 0{\cdot}6$ and above $St_D = 1{\cdot}6$.

The dependence of the jet-column mode of pairing on Re_D is documented in figure 17 for six different cases (*a*) to (*f*), all with initially laminar boundary layers. Cases (*a*)–(*d*) are represented by solid data symbols while the last two are represented by the open symbols. For cases (*a*)–(*d*), where St_θ varied from 0·0025 to 0·011, the subharmonic formation was stable, being evident from the periodic oscilloscope trace of the $\tilde{u}$ signal, and the evolution of the subharmonic for all four cases were essentially

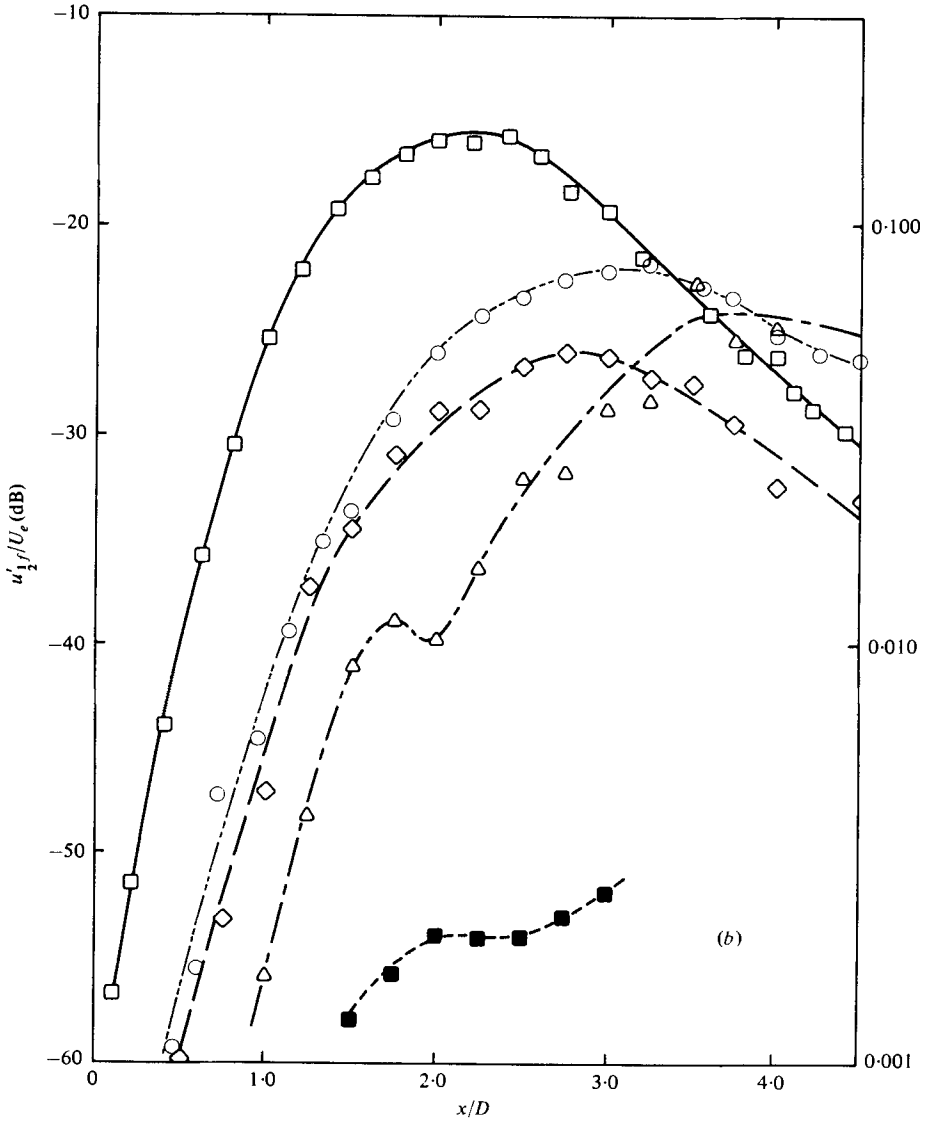

FIGURE 16. (*a*) Evolution of the centre-line spectral amplitudes in the jet column mode; $D = 7{\cdot}62$ cm; $f_p = 70$ Hz; $St_D = 0{\cdot}85$ ($St_\theta = 0{\cdot}0025$); $u'_{ec}/U_e = 3\,\%$. (*b*) Dependence of centre-line $u'_{\frac{1}{2}f}(x)$ on St_D; $D = 7{\cdot}62$ cm; $u'_{ec}/U_e = 3\,\%$; – – –, △, $St_D = 0{\cdot}60$, $Re_D = 4{\cdot}16 \times 10^4$; — · · —, ○, $St_D = 0{\cdot}75$, $Re_D = 3{\cdot}66 \times 10^4$; ——, □, $St_D = 0{\cdot}85$, $Re_D = 3{\cdot}20 \times 10^4$; — —, ◇, $St_D = 1{\cdot}0$; $Re_D = 4{\cdot}3 \times 10^4$; – – – –, ■, $St_D = 1{\cdot}6$, $Re_D = 4{\cdot}3 \times 10^4$.

the same. In the case (*c*), St_θ was 0·0107, thus essentially satisfying both shear-layer and jet-column modes of pairing conditions. This figure thus clearly indicates that the evolution of the subharmonic in the jet-column mode, for initially laminar cases, is independent of St_θ and thus of the shear layer mode.

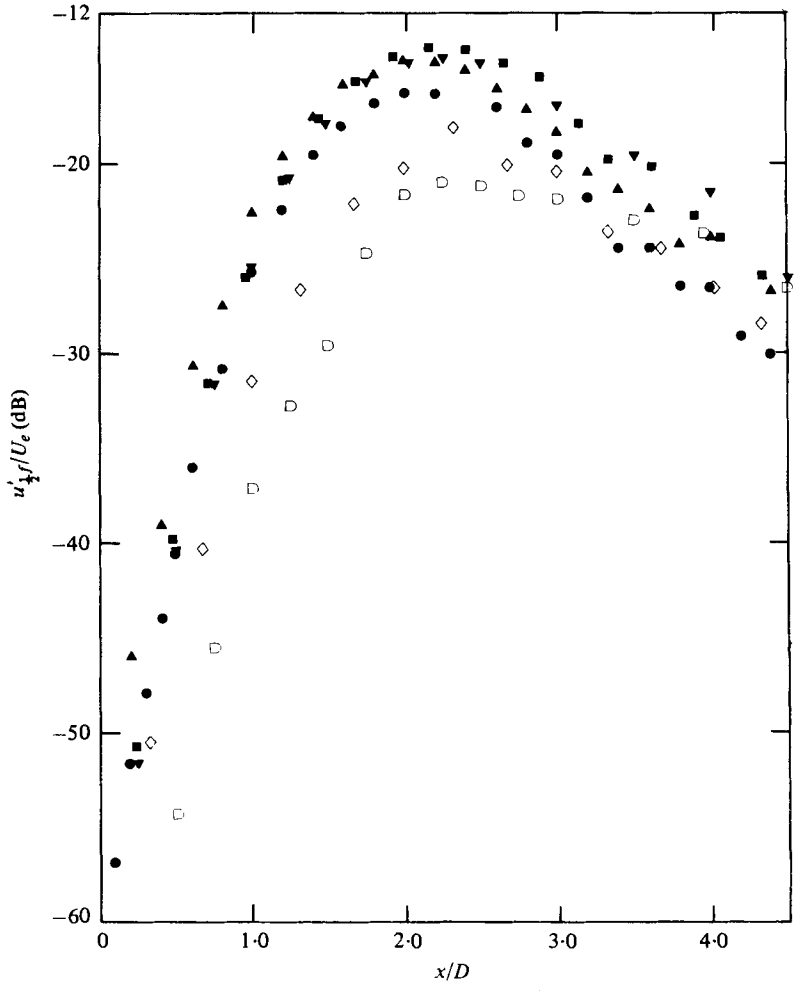

FIGURE 17. Dependence of centre-line $u'_{\frac{1}{2}f}(x)$ on Re_D; $St_D = 0{\cdot}85$.

		Jet diameter (cm)	St_θ	Re_D	f_D(Hz)	u'_{ec}/U_e (%)
(*a*)	●	7·62	0·0025	32000	70	3
(*b*)	■	5·27	0·0047	24000	110	3
(*c*)	▲	2·54	0·0107	8900	174	3
(*d*)	▼	2·54	0·0045	51300	1004	1
(*e*)	D	2·54	0·0034	77600	1520	0·4
(*f*)	◇	7·62	0·002	50600	110	3

3.6. *Effects of Reynolds number and initial condition on pairing*

The last two cases in figure 17 (i.e. cases (*e*) and (*f*)) are at higher Reynolds numbers, and oscilloscope traces of the $\tilde{u}$ signal indicate occasional breakdown and formation of the half-frequency wave form. The time averaged $u'_{\frac{1}{2}f}$ along the jet centre-line in these cases are thus lower everywhere than the first four cases. The $u'_{\frac{1}{2}f}$ peak in the spectrum in those cases when pairing is not stable is no longer a sharp spike, but appears

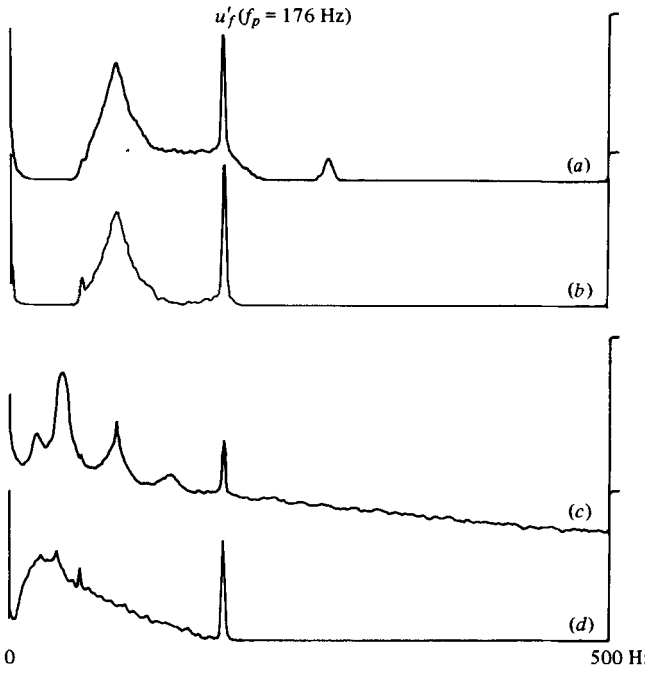

FIGURE 19. Spectra of the $\tilde{u}$ signal at $x/D = 1{\cdot}5$, $y/D = 0{\cdot}30$ in the 7·62 cm jet. Jet-column mode, $St_D = 0{\cdot}85$, $U_e = 15{\cdot}8$ m s^{-1}: (*a*) laminar exit boundary layer; (*b*) tripped. Shear-layer mode, $St_\theta = 0{\cdot}011$, $U_e = 4{\cdot}1$ m s^{-1}; (*c*) laminar exit boundary layer; (*d*) tripped.

as a hump centred at $\frac{1}{2}f_p$ and the peak amplitude is much lower than when the pairing process is stable. Although broadband, this peak is still unambiguous and indicative of the strong tendency of the vortices to pair up.

Two oscilloscope trace pictures of $\tilde{u}$ signal at $St_D = 0{\cdot}85$ are shown in figure 18 (plate 1) for: (*a*) initially laminar and (*b*) initially tripped boundary layers. The regularity of the subharmonic observed in the laminar case in (*a*) is disrupted in the turbulent boundary-layer case (*b*), but a tendency for pairing is still evident. Even during the short intervals the subharmonic formation is complete, the amplitude is not as high as that found for the laminar case (vertical scale of (*a*) is twice that of (*b*)). This, together with the occasional formation and breakdown of the subharmonic, results in a hump in the spectra at $\frac{1}{2}f_p$, but with an amplitude small compared to the stable pairing case (see figures 3*b* and 5*a*).

Figure 19 shows four u spectra in the 7·62 cm jet. Figure 19(*a*, *b*) represent the jet-column mode pairing at $St_D = 0{\cdot}85$. Figure 19(*c*, *d*) are for the shear-layer mode pairing at $St_\theta = 0{\cdot}011$. The Re_D (= 70000) for the laminar case (figure 19*a*) being high, pairing is not stable and the spectrum shows a broad peak at $\frac{1}{2}f_p$. When the boundary layer is tripped, the intermittent pairing process is still evident from the hot-wire trace, and the spectrum is not significantly different in (*b*); $u'_{\frac{1}{2}f}$ peak is only slightly lower than that in figure 19(*a*). Thus, although the stable jet column mode pairing process, found at lower Re_D, is disrupted by tripping, there is evidence of strong pairing activity even with a fully turbulent exit boundary layer. The large random fluctuations in the exit boundary layer of the tripped case, or in the laminar

case but at high Reynolds numbers, appear to cause some jitter in the pairing process downstream. In the latter case, however, tripping has very little further effect on the already intermittent pairing process.

For the shear layer mode pairing, on the other hand, tripping removes the subharmonic peak(s) from the spectrum completely. Notice the occurrence of the spectral peaks at $\frac{1}{2}f_p$, $\frac{1}{4}f_p$ and even $\frac{1}{8}f_p$ in the laminar case (figure 19*c*), while for the tripped case in (*d*) none of these peaks are present. This is not unexpected; tripping presumably pre-empts the exit shear-layer instability. The initially turbulent boundary layer may still roll up, but this roll-up process is likely to be quite different from the laminar shear-layer roll-up and probably occurs sufficiently farther downstream (Hussain & Zedan 1978; Clark 1979).

The jet-column mode of vortex pairing with initially turbulent boundary layer is further demonstrated in figure 20(*a*). This figure corresponds to the conditions in figure 13(*d*) but with tripped exit boundary layer, both figures are for the same probe location, $x/D = 1{\cdot}5$ and $y/D = 0{\cdot}30$. While $u'_f(U_e)$ remains essentially unchanged, the sharp peaks in the $u'_{\frac{1}{2}f}$ variations are no longer present in figure 20(*a*). Notice the complete disappearance of the $u'_{\frac{1}{4}f}$ peak at the shear-layer mode condition while $u'_{\frac{1}{2}f}$ unambiguously peaks up at the velocity ($U_e \simeq 9{\cdot}5$ m s^{-1}) corresponding to the jet-column mode of excitation. Similar results were obtained with the 2·54 cm tripped jet and at different excitation frequencies but are not shown. The dependence of $u'_{\frac{1}{2}f}(x)$ on St_D is shown in figure 20(*b*) for the tripped 2·54 cm jet with Re_D kept constant at 51 000. Operation at a constant but high Re_D (thus assuring fully turbulent state of the exit boundary layer) was desired; this, along with the available excitation frequencies, governed the limited choice of the St_D's. For $St_D = 0{\cdot}8$, 0·85 and 1·13, there were unambiguous humps at $\frac{1}{2}f_p$ in the spectra in the range $x/D < 4$. But for $St_D \simeq 0{\cdot}44$, the spectrum did not have an identifiable peak or even a hump at $\frac{1}{2}f_p$ anywhere in x; the figure shows the amplitude read from the spectrum at $\frac{1}{2}f_p$. The larger growth rate and larger $u'_{\frac{1}{2}f}$ at $St_D = 0{\cdot}85$ clearly show the strongest tendency for pairing at this Strouhal number even when the exit boundary layer is turbulent.

The above results thus lead to the belief that the jet column mode is independent of the shear layer characteristics; the jet-column mode is neither a legacy of the shear-layer mode nor is its formation dependent on the latter.

3.7. *Flow visualization experiments*

Inference of the coherent structure from the hot-wire signal is not always unambiguous. It is therefore desirable that solid evidence in the form of visualization pictures should be obtained in conjunction with hot-wire data. Two streaks of smoke emerging along the shear layer, when viewed normal to the plane containing the streaks and the jet centre-line gave the cross-sectional view of the jet. A stroboscope was used to illuminate the flow at the excitation frequency or at any of its subharmonic frequencies. By adjusting the phase of the strobe trigger, the 'frozen' structure could be shifted in x as desired so that spatial and temporal development of the vortices could be observed. The camera shutter speed was adjusted so that only one flash occurred while the shutter remained open; the duration of illumination was about 2 microseconds. This way, 'instantaneous' pictures were obtained at desired phases of the events of interest.

Figure 21 (plate 2) shows the unexcited jet structure at $Re_D = 32\,000$. No vortical

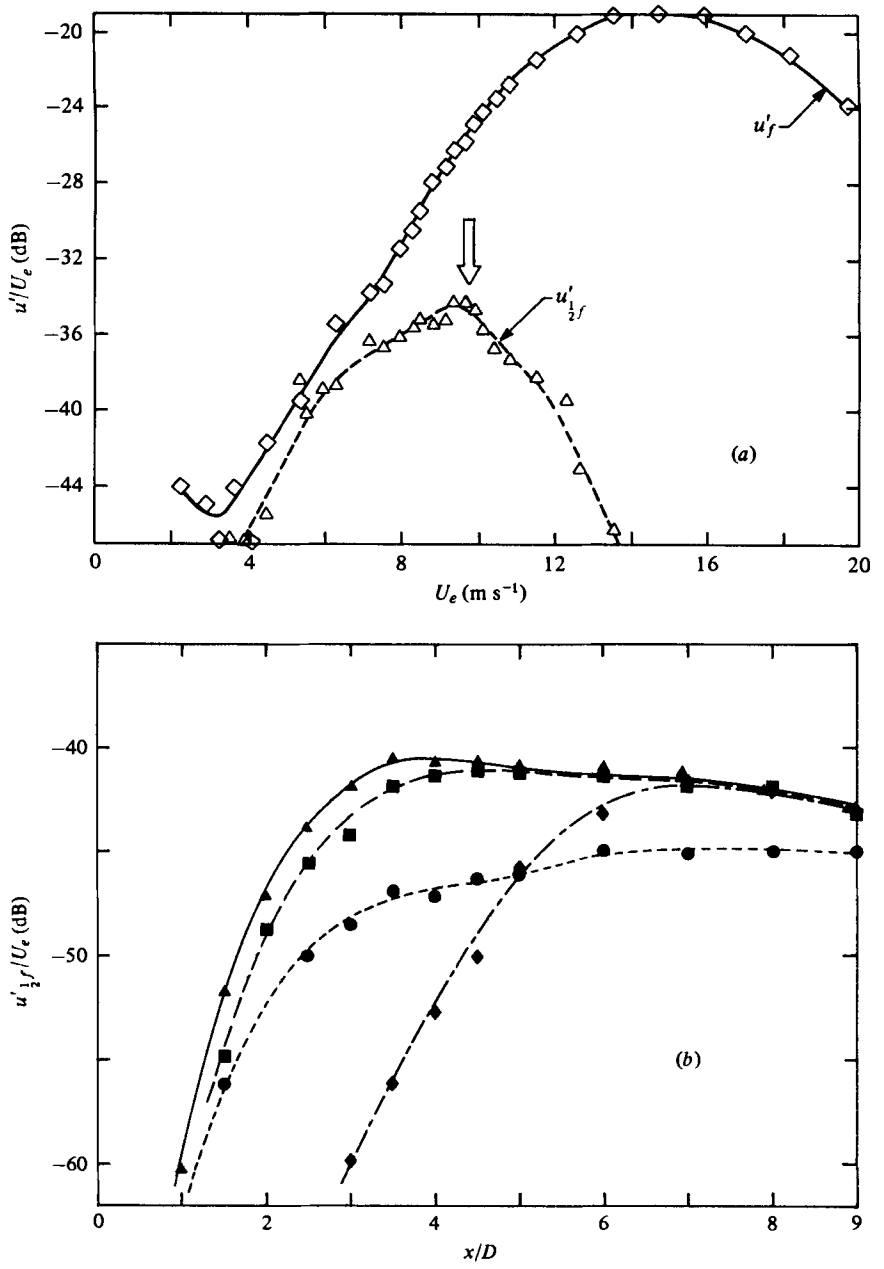

FIGURE 20. (*a*) Dependence of u'_f and $u'_{\frac{1}{2}f}$ on U_e in the 7·62 cm tripped jet. Measurement conditions same as in figure 13(*d*). (*b*) Dependence of centre-line $u'_{\frac{1}{2}f}(x)$ on St_D for the 2·54 cm tripped jet. $Re_D = 51000$; $u'_{ec}/U_e = 1\,\%$. St_D values are: ◆, 0·44; ■, 0·80; ▲, 0·85; ●, 1·13.

structure similar to Brown & Roshko's (1974) 'roller structure' is apparent. High-speed flow-visualization movies in the mixing layer of a circular jet in our laboratory (Clark 1979) revealed that with increasing Reynolds numbers, the mixing layer progressively becomes disorganized. The smoke traces in such a case may occasionally reveal an organized train of vortices but most of the time do not show any structure.

It is possible that the latter state is captured in figure 21. Also, flow-visualization pictures in the present study were meant to provide qualitative descriptions and were not optimized to produce high-contrast pictures in each case.

Figure 22(*a*, *b*) (plate 3) shows the jet-column mode pairing (at $St_D = 0{\cdot}85$ and $Re_D = 32000$) at two different phases. Following the roll-up at $x/D \simeq 0{\cdot}3$, the radial configuration of the two pairing vortices occur at $x/D \simeq 1{\cdot}5$. Beyond $x/D = 4$, the smoke traces become too diffuse to clearly show any orderly structure. The shear-layer mode of pairing (at $St_\theta \simeq 0{\cdot}012$) is captured in figure 23(*a*, *b*) (plate 4) for two different Re_D. While in figure 23(*a*) only one stage of pairing can be detected due to the smoke traces getting too diffuse farther downstream, picture (*b*) at a lower speed clearly shows a second stage of pairing. Figure 23(*b*) corresponds to the shear-layer mode peak condition in figure 13(*d*). At a number of excitation situations which do not satisfy either of the conditions $St_D = 0{\cdot}85$ or $St_\theta \simeq 0{\cdot}012$, no evidence of pairing can be observed (figure 24, plate 5). However, if any of the two conditions are nearly satisfied (say, at $St_D = 0{\cdot}6$ or $1{\cdot}2$), occasional pairing was observed.

Comparison of figures 22 and 23 reveals some kinematic differences between the shear layer and the jet column mode pairings. The shear layer mode pairing appears similar to that in a single free shear layer, flow-visualization pictures of which can be found in many previous works (e.g. Freymuth 1966; Rockwell 1972; Winant & Browand 1974). Shortly before pairing in this mode, the cross-section of the two thin vortices deform and the two together roughly form a circle with an S-shaped demarcation still identifying the two vortex cores. This demarcation between the two cores is soon lost and the resulting paired vortex may still maintain a quasi-laminar structure before the next stage of pairing (see figure 23*b*). On the other hand, in the jet column mode, the cores maintain more or less circular cross-sections, except that the cross-section of the inner one gets somewhat elongated (figure 22), and mingling of the vortical fluid from the two cores appears to begin only when the inner vortex is ahead of the outer one, after having passed through the latter in a leap-frog fashion. Pairing in the shear layer mode is similar to that in a plane shear layer and thus not pursued further; a typical case of pairing in the jet column mode was chosen for detailed studies.

3.8. *Pairing process, vortex trajectories and convection velocities*

The following measurements were carried out in the 7·62 cm jet at $St_D = 0{\cdot}85$, $Re_D = 32000$, with the exit excitation level $u'_e/U_e = 3\ \%$. The exit flow characteristics were laminar (see § 3.1).

The two pairing vortices at two phases of the pairing process have been shown in figure 22. The two vortices start attaining distinctly different characteristics starting from $x/D \simeq 0{\cdot}5$. One of them (say, vortex 1) starts shrinking in its toroid diameter while beginning to accelerate. The other (say, vortex 2) begins to dilate and decelerate, thus allowing the vortex 1 to catch up with it and pass through its interior in a leap-frog motion. At $x/D \simeq 1{\cdot}5$, the two vortices attain the radial configuration; i.e. vortex 1 is inside vortex 2, both located in a plane perpendicular to the jet axis. Immediately after the radial configuration, the vortex 1 is seen to undergo a violent transition resulting in sudden diffusion of the smoke traces; its centre, however, is still identifiable as a knot of diffuse smoke for some distance farther downstream. Vortex 2 on the

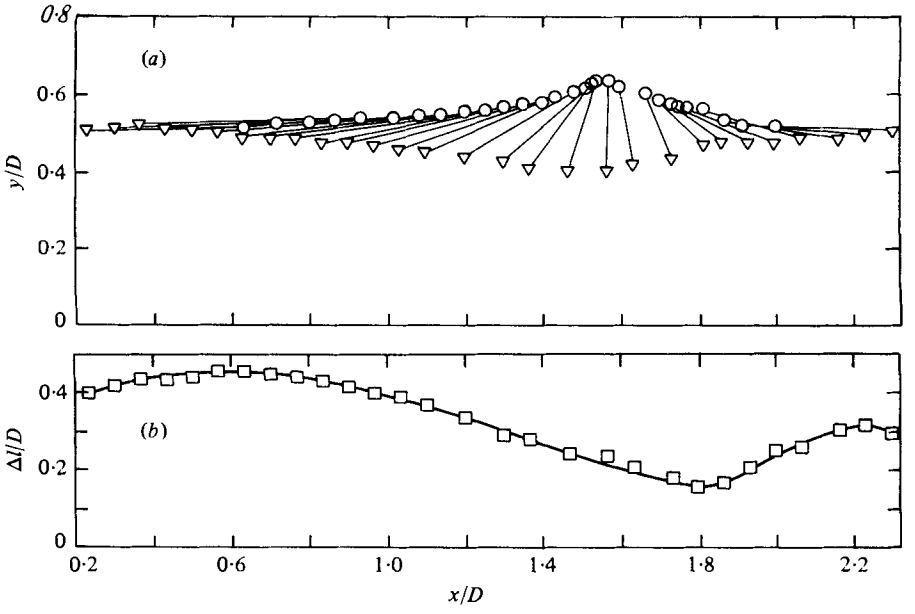

FIGURE 25. Vortex pairing in the 7·62 cm jet at $St_D = 0{\cdot}85$, $Re_D = 32000$, $u'_{ec}/U_e = 3\,\%$; (*a*) trajectories, (*b*) separation distance.

other hand, maintains its quasi-laminar structure approximately up to $x/D = 2$. Beyond $x/D \simeq 1{\cdot}5$, the vortex 1 is ahead of the vortex 2, and its diffuse smoke traces appear to unwind and wrap around the periphery of the latter. Beyond $x/D \simeq 2{\cdot}5$, the two vortices are no more identifiable as separate entities. Around $x/D = 2{\cdot}5$, traces of diffuse smoke are seen to sprout out in a large-scale violent motion. This is apparently associated with evolution of azimuthal secondary structures, three-dimensionality and turbulent breakdown (Yule 1978; Davies & Baxter 1978). The cross-section of the paired vortex becomes progressively more diffuse as the structure travels downstream. Beyond $x/D \simeq 4$, the smoke does not reveal any structure. (Alternative techniques to visualize the flow further downstream failed.)

A needle mounted on an x–y traverse mechanism was used to locate accurately the centres of the vortices at different stroboscopically frozen locations (i.e. phases) and the trajectories are shown in figure 25(*a*). The centres of the two pairing vortices at each phase are joined by a line. Thus if one considers a diametral plane cut through one side of the two vortices and defines a dumb-bell with the two vortex cross-sections at its ends, then figure 25(*a*) shows the motions of this dumb-bell as the vortex pair undergoes the leap-frog motion and merger while moving downstream. A line connecting the triangular data points will thus be the phase-average trajectory of the centre of vortex 1 and the line through the circular data points, that of the centre of vortex 2. The curve in figure 25(*b*) shows the spacing of the centres of the two vortices (or the dumb-bell axis length) as a function of the axial location of vortex 1. Note that minimum spacing occurs shortly after the radial configuration where the vortex 1 is seen to undergo an explosive transition. From this latter axial location onward, while smoke traces from vortex 1 wraps around vortex 2, the still identifiable centre of the former is seen to recede from the latter; this is indicated by the increase in $\Delta l(x)$ after $x/D \simeq 1{\cdot}75$.

A phase-locked flow-visualization technique was adopted for determining the convection velocities of the two types of vortices during the pairing event. The signal from a single hot-wire probe 1 (on the jet centre-line and at $x/D > 1{\cdot}5$) was band-pass filtered to obtain a sinusoidal signal at frequency $\frac{1}{2}f_p$. This probe 1 signal was used to trigger the stroboscope to illuminate the flow. Translation in x of this probe 1 changed the phase of the $\frac{1}{2}f_p$ signal with respect to a fixed reference probe 2 signal (also band-passed at $\frac{1}{2}f_p$). The phase changes were read using a lock-in-amplifier, tuned at the frequency $\frac{1}{2}f_p$. The centre of a particular vortex was made to coincide with one of two stationary needles, separated in x at a fixed $\Delta x = 1$ cm, the phase reading in the lock-in-amplifier was noted, and then probe 1 was translated in x to get the same vortex centre coinciding with the second needle. The new phase reading gave $\Delta\phi$ from which the longitudinal convection velocity v_x was calculated, via $d\phi/dx \simeq \Delta\phi/\Delta x = 2\pi/\lambda$. This value of v_x for the particular vortex (centre) was assigned to the x location midway between the two needles. The pair of needles was then translated in x by 0·5 cm and the procedure repeated to obtain v_x of the particular vortex 0·5 cm downstream.

The values v_x/U_e for the two types of vortices are plotted in figure 26(*a*) as function of x/D for $x/D \lesssim 4$. Note that the above-mentioned phase-locked visualization technique has been used to obtain the data up to $x/D = 2{\cdot}25$; the individual identities of the two vortices farther downstream is lost, and v_x in this region was computed by phase-locked measurements, based on analog signals, by treating each paired vortex as a single one constituting a convecting street. These data show that both the vortices accelerate after roll-up, then vortex 1 continues to accelerate but vortex 2 starts decelerating. At $x/D \simeq 1{\cdot}5$, the former reaches its peak convection velocity while the latter reaches its lowest. At this point vortex 1 has a velocity even higher than the jet-core mean velocity, by about 25 %, while vortex 2 velocity is about one fourth that of vortex 1. The little knot in the convection velocity curves (figure 26*a*) after $x/D = 2$ is not unambiguous but can be ascribed to the continued 'leap-frogging' tendency between the two vortices. The average value of v_x/U_e for the paired vortex is about 0·56 and remains approximately constant within the distances measurements could be made. This convection velocity is somewhat lower than $0{\cdot}72\,U_e$ found by Yule (1978) in an axisymmetric mixing layer and $0{\cdot}68\,U_e$ found by Sokolov *et al.* (1980) for a spark-induced 'spot' in a mixing layer, but in close agreement with the data of Ko & Davies (1971), Lau, Fisher & Fuchs (1972), Bradshaw, Ferriss & Johnson (1964) and Petersen (1978). Also, from space–time trajectories of large-scale structures in a high Reynolds number mixing layer, Hussain & Clark (1980) deduced a structure convection velocity of $0{\cdot}60\,U_e$.

The dashed lines in figure 26(*a*) represent convection velocity curves for pairing ring vortices in a circular water jet at $Re_D = 5000$ (Browand & Laufer 1975), calculated from position–time information of successive ciné-film frames. There are large differences between these and the present data. For example, the axial location where the inner and the outer vortices reach maximum velocity difference shortly before amalgamation is about $2{\cdot}5D$ instead of $1{\cdot}5D$ found in the present study. These differences could be due to a number of reasons. The vortex pairing in the present study is an organized phenomenon (organized by controlled excitation). This essentially eliminated jitter in the pairing process itself and also in its spatial location in an unexcited jet.

The Reynolds number (Re_D) value of 5000 in Browand & Laufer's experiment was

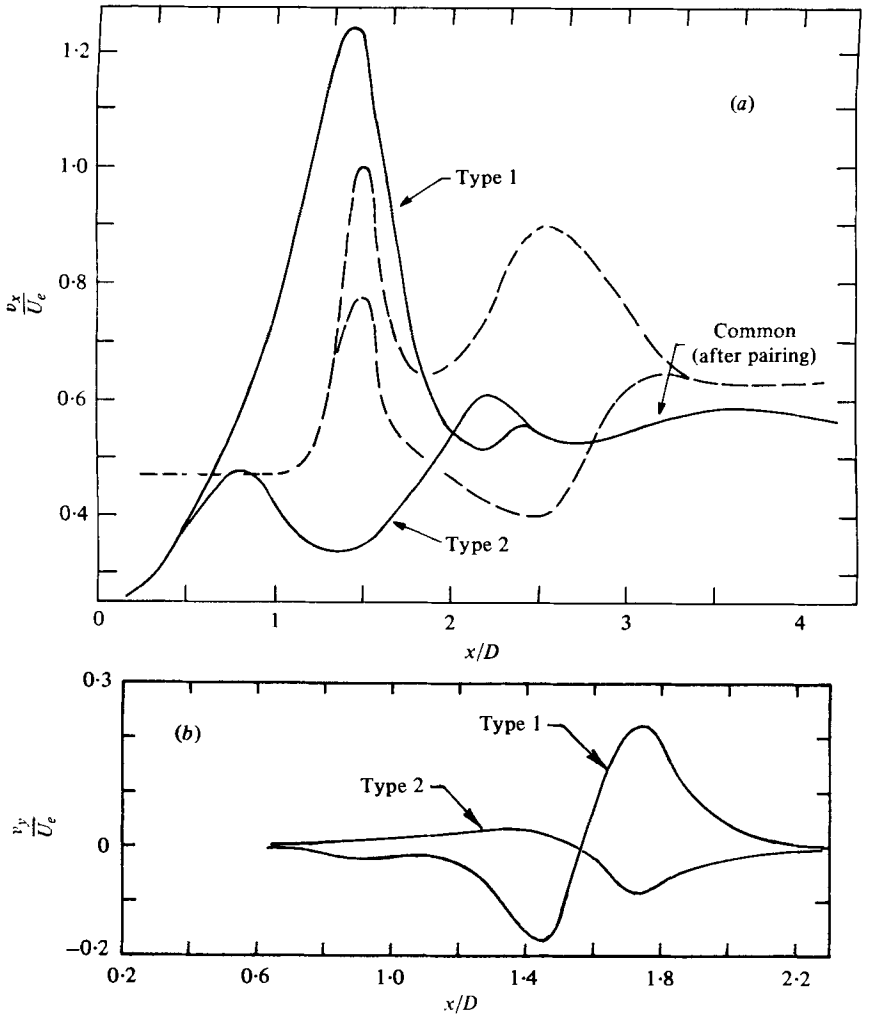

FIGURE 26. (*a*) Longitudinal and (*b*) transverse convection velocities of the two pairing vortices. ———, data of Browand & Laufer (1975).

much lower than 32000 in the present study. Davies & Baxter (1978) have shown that when Re_D falls below 7000 the initial growing waves become elongated and take 2 to 3 wavelengths (λ) before roll-up while at higher Re_D it takes about $1{\cdot}5\lambda$. They also showed that the most unstable wavelength λ_0 follows the Rayleigh criterion $\lambda_0/D = 24\sqrt{Re_D}$ so that with increasing Re_D, the roll-up will occur progressively closer to the lip. Becker & Massaro (1968) showed that the roll-up length L from the lip is given as $L/D = 107/\sqrt{Re_D}$. Since their data were obtained with a jet of a fixed diameter, thus taking D as a constant, it is clear that with higher Re_D or U_e the location of roll-up and thus subsequent pairing will move upstream. (Becker & Massaro observed the pairing to occur at 5λ downstream from the lip.) This would explain why the location of maximum relative velocity occurs at a larger x/D in Browand & Laufer's (1975) data.

Another factor may be the flow configuration in Browand & Laufer's experiment,

which consisted of a confined jet, the nozzle being axisymmetrically mounted in a cylindrical tank which was 11 times the jet diameter in width and 30 jet diameters in length. It is probable that in this flow, the confinement effect is non-negligible (Becker & Massaro 1968).

The transverse convection velocity $v_y(x)$ for the two vortices during pairing is shown in figure 26(*b*). Note that the radial velocities for the two vortices are everywhere opposite in sign and each changes sign roughly at the location of the radial configuration. Note also that vortex 1 undergoes large radial acceleration at $x/D \simeq 1{\cdot}5$.

3.9. *Time-average field measurements*

Time-average measurements in the presence of controlled vortex pairing are reviewed and compared with the corresponding unexcited jet data. Although these data do not capture the details of the vortex pairing dynamics, they document modification of the average measures of the flow by the controlled pairing phenomenon.

In figure 27(*a*, *b*), contours of constant u' and v', respectively, are shown for $St_D = 0{\cdot}85$ and $x/D \leqslant 5$. Note that the scales for the ordinate are magnified 3·75 times the abscissa. Also included in the u' contours are the trajectories of the two pairing vortices (figure 25). The trough region (i.e. local valley) in the u' contours centred around $x/D = 1{\cdot}5$ and $y/D = 0{\cdot}5$ falls between the trajectories of the two pairing vortices; the v' contours show unimodal distributions at this location. The different trends in the u' and v' distributions at this location can be qualitatively explained by the induced motions of the vortices. Consider the probe to be located in the middle of the trough region in u' contours at $x/D \simeq 1{\cdot}5$; the variation in the $\tilde{u}(t)$ signal observed during the passage of the vortex pair will be less since the axial components of the velocities induced by the two vortices will cancel each other. On the other hand, the transverse components of the induced velocities will mostly add, thus the intense relative motions of the two vortices at this location will produce large $\tilde{v}(t)$ variations.

Figure 28(*a*, *b*) shows the constant $\overline{uv}$ contours for $x/D \leqslant 5$ for $St_D = 0$ and 0·85, respectively. These time-average plots, while not capturing the details of vortex pairing, do still illustrate the changes in the turbulence structure brought about by the organized pairing process under excitation. Figure 29 shows the streamwise variations of the peak value of $\overline{uv}$ for $St_D = 0$ and 0·85. Of the two peaks of $\overline{uv}$ for $St_D = 0{\cdot}85$, the first one appears to be associated with the roll-up process and the second, at $x/D \cong 1{\cdot}5$, with the intense pairing process. Since under controlled pairing, a particular phase of the pairing event occurs also at a particular spatial location, the second peak in $\overline{uv}_{\max}(x)$ located at $x/D \cong 1{\cdot}5$ indicates that the 'average correlation' may be higher at a particular phase of the pairing process. This is indeed observed in the phase-average measurements (part 2). For $x/D \gtrsim 2$, the time-average peak $\overline{uv}$ values for the $St_D = 0{\cdot}85$ case are not significantly different from those for $St_D = 0$.

It should be noted that the peaks of the profiles of $u'(y)$, $v'(y)$, and $\overline{uv}(y)$ in the unexcited axisymmetric shear layer occur towards the high-speed side of the layer at locations where U/U_e values are about 0·6, 0·7 and 0·67, respectively. The widths of the profiles of u', v', and $\overline{uv}$ are not equal; the width of the first is the largest and that of the third the smallest. When excited at $St_D \simeq 0{\cdot}85$, as a result of organized transverse motions of the vortices during pairing, the profiles $u'(y)$ and $\overline{uv}(y)$ become bimodal around $x/D \simeq 1{\cdot}5$.

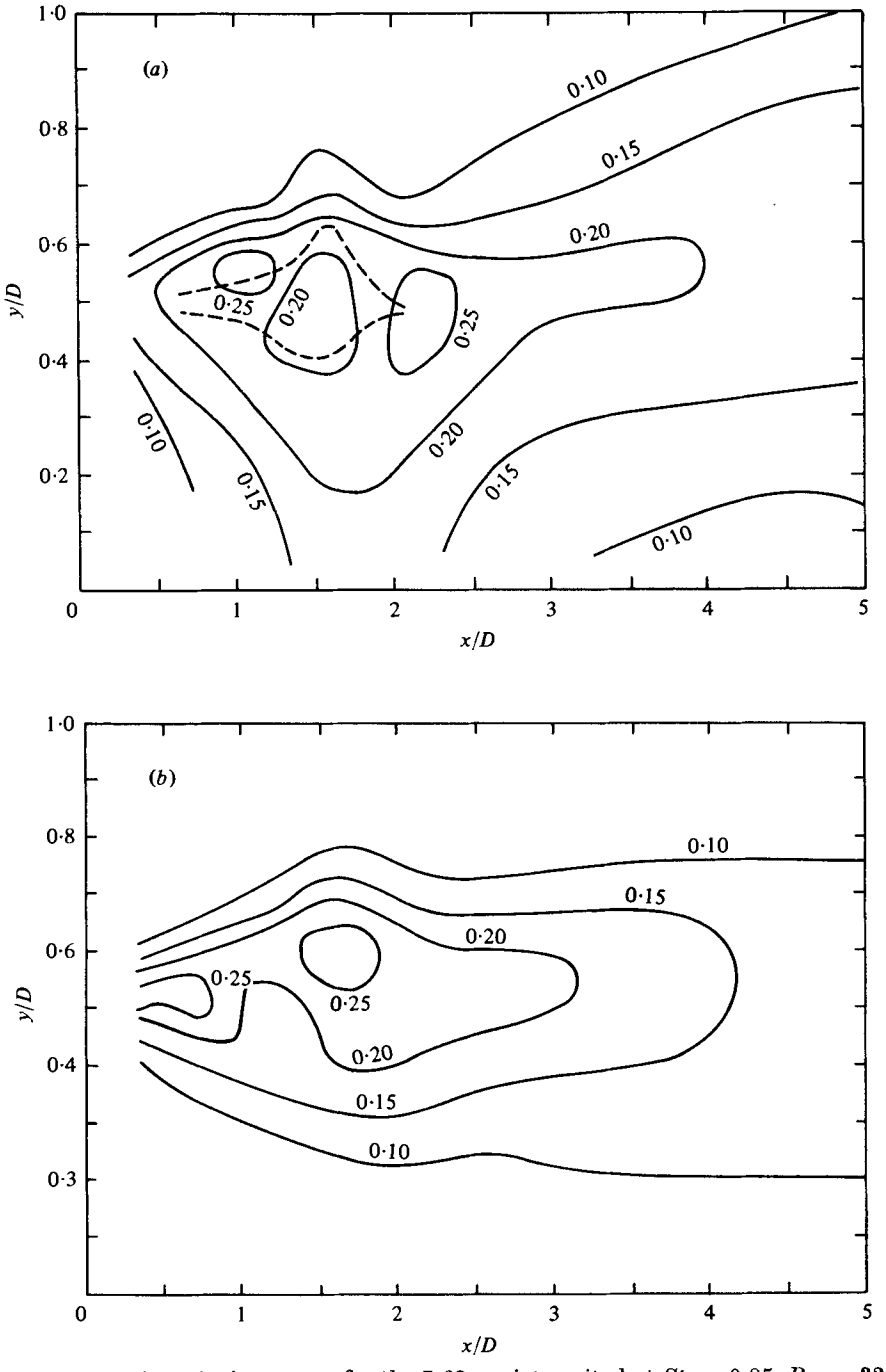

FIGURE 27. u', v' contours for the 7·62 cm jet excited at $St_D = 0{\cdot}85$, $Re_D = 32000$, $u'_{ec}/U_e = 3\,\%$. (*a*) u'/U_e; (*b*) v'/U_e.

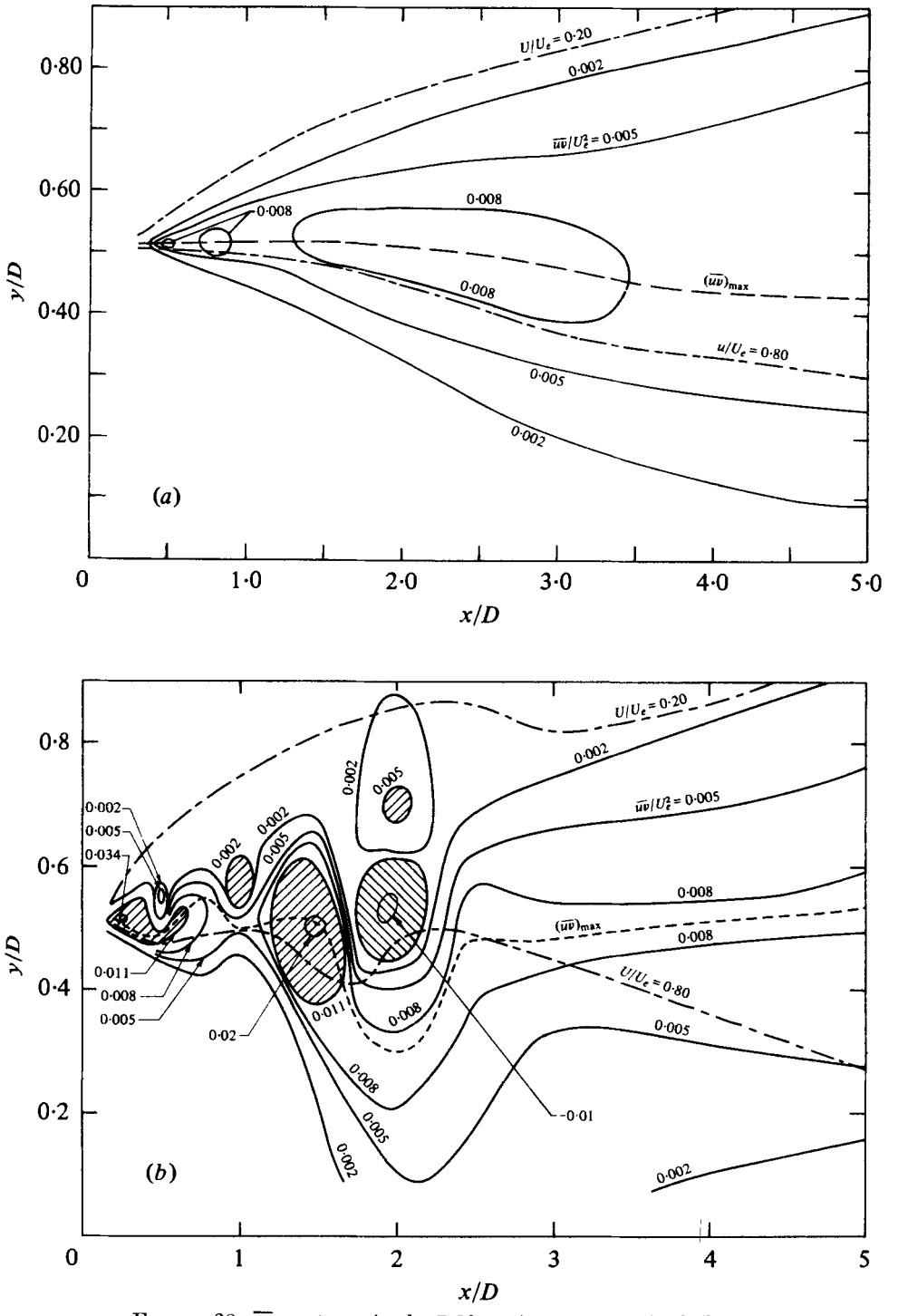

FIGURE 28. $\overline{uv}$ contours in the 7·62 cm jet: (*a*) unexcited, $Re_D = 32000$. (*b*) $St_D = 0{\cdot}85$, $Re_D = 32000$, $u'_{ec}/U_e = 3\,\%$. ▨, peak $(\overline{uv})$; ▧, negative $(\overline{uv})$.

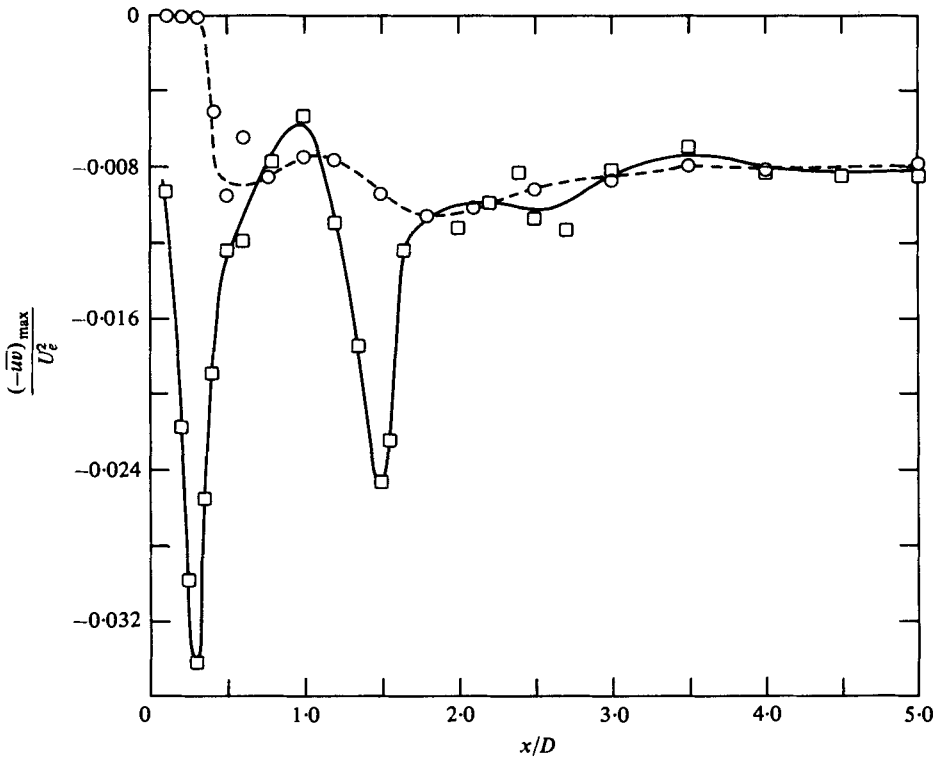

FIGURE 29. Variation of the $-\overline{uv}$ peak with x at $Re_D = 37000$ in the 7·62 cm jet; – – – –, $St_D = 0$; ——, $St_D = 0{\cdot}85$, $u'_{ec}/U_e = 3\,\%$.

In the absence of controlled excitation, the formation and interaction of the coherent structures are random and consequently their effect is smoothed out in a time-average map. In our specific case of controlled excitation, the formation and interaction are stabilized in space and time so that each phase of the pairing process occurs at a particular location at periodic intervals. That is why the time average will retain some features of the coherent structure interactions (figure 28*b*). Note also the noticeable average flow distortion, for example the locations of U/U_e = constant and $\overline{uv}_{max}$ lines, recorded in figure 28(*b*) as opposed to those in figure 28(*a*). Thus, the excitation effectively thickens the shear layer by localizing the coherent structure interactions.

Note that at $x/D \simeq 2$ in the middle of the excited shear layer, the time-average Reynolds stress is negative (the maximum negative value of $\overline{uv}/U_e^2$ being 0·01), thus indicating locally negative (i.e. counter-gradient) production over a significant spatial region.† Over this region, u' has a local minimum, as to be expected from the negative production. Because of relatively poorer resolution, the v' data do not clearly indicate (but allows the possibility of) a local minimum over the same region. The time-average profile $U(y)$ over this region is monotonic, like that in the unexcited flow, except that it is wider for the excitation. The negative production, confirmed through repeat measurements, is clearly in contrast with the gradient transport hypotheses

† Subsequent to our study, Wygnanski, Oster & Fiedler (private communication) have observed negative production in a strongly forced plane mixing layer. For a discussion of negative production in turbulent shear flows, see Beguier *et al.* (1978).

as well as turbulence modelling theories, but can be explained on the basis of coherent structure motions (see part 2: Hussain & Zaman 1980; Hussain, Kleis & Sokolov 1980). Especially during pairing, the interacting and advecting coherent structures can produce Reynolds stress with its sign alternating in space and time. The time-average Reynolds stress can be of either sign.

Figure 30(*a*, *b*, *c*) (plate 6) shows the traces of the instantaneous signals $\widetilde{uv}(t)$ (bottom) and $\tilde{u}(t)$ (top) at $x/D = 0{\cdot}3$, $0{\cdot}6$, and $1{\cdot}75$, respectively, each for the y location where $\overline{uv}$ is maximum. The $\tilde{u}$ signal, apart from capturing the details of the vortex structure, shows the evolution of the half-frequency during pairing. At each station, while the average values may not be large, the $\widetilde{uv}$ signal shows large excursions. That is, the effect of controlled excitation is much more dramatic than revealed in time average data (figures 28*a*, *b*). A measure of the signal excursion can be obtained from the standard deviation σ_{uv} of the $\widetilde{uv}(t)$ signal. The transverse profiles of σ_{uv}, are shown in figure 31(*a*) for $St_D = 0$ and $0{\cdot}85$ at $x/D = 1{\cdot}75$; note that

$$\delta_\omega = U_e/(\partial U/\partial y)_{\max}.$$

The two peaks for $St_D = 0{\cdot}85$ occur nearly at the same locations where $\overline{uv}$ shows peaks. Note that at $(y - y_{0{\cdot}5})/\delta_\omega = -0{\cdot}4$, the r.m.s. value of $\widetilde{uv}(t)$ under excitation is about 3 times that in the absence of excitation. It is evident that although $\overline{uv}$ may not be large, the excursions in $\widetilde{uv}(t)$ are larger everywhere in the transverse direction during pairing as compared to the unexcited jet. The lower value of σ_{uv} for the excitation case on the low-speed side does not reflect a decrease in Reynolds stress production, but rather, an inward shift towards the jet axis of the coherent structures when the jet is excited, consistent with the $\overline{uv}$ maps in figure 28.

The characteristic large excursions of $\widetilde{uv}$ in the jet when it is excited is best captured in figure 31(*b*) which shows the streamwise variations of the standard deviation σ_{uv}, along the y locations where $\overline{uv}$ is maximum (i.e. same y locations used in figure 29). It is clear that the excursions of the $\overline{uv}$ signal are larger for the $St_D = 0{\cdot}85$ case than for the corresponding unexcited jet. The contours of constant σ_{uv} are shown in figure 31(*c*); note that the region for large excursions of Reynolds stress is limited to the region $0{\cdot}5 \leqslant x/D \leqslant 3{\cdot}0$, but spread over a wider extent in the transverse direction at the location of vortex pairing, i.e. at $x/D \simeq 1{\cdot}75$.

4. Concluding remarks

Hot-wire and flow-visualization studies show that controlled velocity perturbations can remarkably affect the near-field flow of a circular jet. These effects, typically visualized as organization of the coherent structure, can produce large augmentation as well as suppression of turbulent velocity fluctuations depending on the Strouhal number, Reynolds number and initial flow state, i.e. laminar or turbulent. The value $St_D = 0{\cdot}3$ can still be regarded as the 'preferred mode' of a jet if redefined to be based on the centre-line fundamental amplitude rather than total centre-line fluctuation intensity. Large augmentation of velocity fluctuation has been shown to be associated with vortex pairing in the jet. Turbulence suppression occurs at $St_D \simeq 1{\cdot}6$, which is quite different from the value $2{\cdot}75$ found by Vlasov & Ginevskiy (1974); this phenomenon needs investigation. Spectral evolution of velocity fluctuation during pairing,

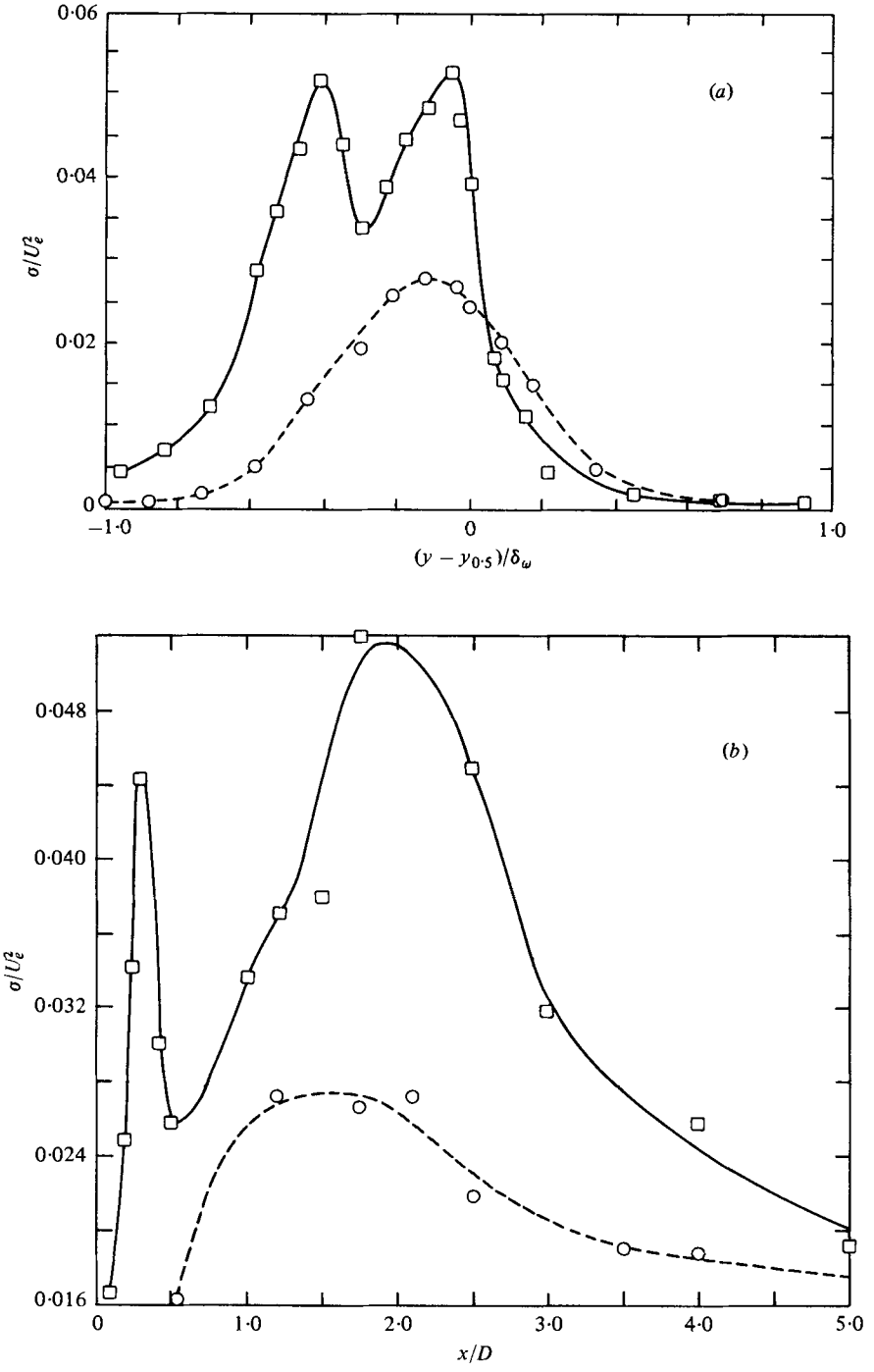

FIGURE 31 (*a*, *b*). For legend see facing page.

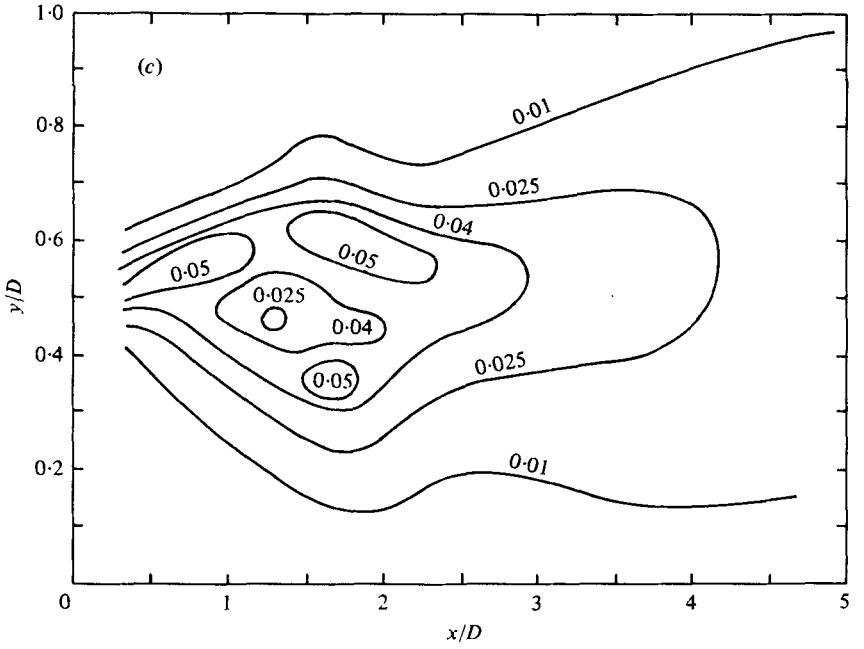

FIGURE 31. (*a*) $\sigma_{uv}(y)$ at $x/D = 1{\cdot}75$ in the 7·62 cm jet at $Re_D = 32000$: ——, $St_D = 0{\cdot}85$, $u'_{ec}/U_e = 3\,\%$; – – – –, $St_D = 0$. (*b*) $\sigma_{uv}(x)$ corresponding to the y location of data in figure 29; $D = 7{\cdot}62$ cm; $Re_D = 32000$; – – – –, $St_D = 0$; ——, $St_D = 0{\cdot}85$. (*c*) σ_{uv} contours; $D = 7{\cdot}62$ cm; $St_D = 0{\cdot}85$; $Re_D = 32000$; $u'_{ec}/U_e = 3\,\%$.

the conditions most favourable for vortex pairing, and the details of flow dynamics during vortex pairing have been documented.

It is shown that vortex pairing in circular jets occurs in two distinct modes: (i) the shear layer mode, i.e. at $St_\theta \simeq 0{\cdot}012$ and (ii) the jet column mode, i.e. at $St_D \simeq 0{\cdot}85$. The excitation frequency corresponding to the shear layer mode approximately matches the natural shear layer roll-up, the corresponding value of St_θ ($\simeq 0{\cdot}012$) being noticeably lower than the most unstable mode frequency ($St_\theta \cong 0{\cdot}017$) predicted by spatial stability theory (Michalke 1965; Miksad 1972).

Browand & Laufer (1975) hypothesized that the large-scale structure formed downstream of the potential core results from (laminar) initial shear layer instability through necessary number of stages of pairing. However, this would not explain Crow & Champagne's observed vortex 'puffs' at $St_D = 0{\cdot}30$ even in an unexcited round jet with turbulent exit boundary layer. If indeed there is a second (i.e. jet-column) mode of instability, the mechanism for selection of this mode must also be considered. It is likely that the exit shear-layer instability mechanism is not always important in determination of the downstream coherent structure. The larger rings involved in the jet-column mode of pairing are not results of pairing of the initial thinner rings; an arbitrary number of these thin vortices are wrapped up together during the roll-up of a shear layer into larger rings. This study should also caution that instability studies of a free shear layer done in a circular jet may not produce unambiguous results due to coupling of the jet column mode with the shear layer mode.

Only one jet-column mode pairing could be observed while the shear layer mode was

found to involve as many as three stages of pairing, the number of stages being higher at higher initial St_D. The jet-column mode pairing was found to be 'stable' at lower Reynolds numbers ($Re_D \lesssim 50000$). At higher Re_D, or with tripped exit boundary layers, the pairing phenomenon is intermittent due to occasional disruption of the pairing process. The trajectories of the pairing vortices and their convection velocities have been documented through phase-locked flow visualization. Differences with similar convection velocity data by Browand & Laufer (1975) have been explained.

Time-average Reynolds-stress distributions during a typical case of jet-column mode of pairing was found to remain unchanged from the unexcited jet for $x/D > 2$, while large values are encountered at $x/D = 0{\cdot}3$ and $1{\cdot}5$. The first peak is believed to be associated with the initial laminar roll-up process, and the second peak at $x/D = 1{\cdot}5$ is related to intense relative motions of two toroidal vortices during the pairing process. The $\widetilde{uv}(t)$ signal traces showed larger 'excursions' everywhere in the flow field for the excited case as compared with the corresponding unexcited case. Especially in the region $1 < x/D < 3$, within which the pairing process is completed, σ_{uv} is very large, indicating that still larger excursions are experienced during the passage of the pair of interacting vortices. Vortex pairing induced by controlled excitation can cause negative production, which contrasts gradient transport hypotheses and turbulence modelling theories, but can be explained on the basis of coherent structures (see part 2, Hussain & Zaman 1980).

Part 2 (Hussain & Zaman 1980) will focus on the experimental and analytical considerations in the study of coherent structure physics in general and then cover the eduction of coherent structure details through phase-locked measurements and examine vorticity, circumferential coherence and coherent and background Reynolds stresses preceding, during and following a pairing event in the circular jet.

This research was funded by the Office of Naval Research under Grant N00014-76-C-0128 and the N.A.S.A. Langley Research Center under Grant NSG-1475. The authors are thankful to S. J. Kleis and L. S. G. Kovasznay for careful reviews of the draft and to them and F. K. Browand and J. Laufer for illuminating discussions on the results.

REFERENCES

Bechert, D. & Pfizenmaier, E. 1975 *J. Sound Vib.* **43**, 581.

Becker, H. A. & Massaro, T. A. 1968 *J. Fluid Mech.* **31**, 435.

Beguier, C., Giralt, F., Fulachier, L. & Keffer, J. F. 1978 *Structure and Mechanisms of Turbulence II* (ed. H. Fiedler), Lecture notes in Physics, vol. 76, p. 22. Springer.

Bradshaw, P., Ferriss, D. H. & Johnson, R. F. 1964 *J. Fluid Mech.* **19**, 591.

Browand, F. K. 1966 *J. Fluid Mech.* **26**, 281.

Browand, F. K. & Laufer, J. 1975 *Turb. Liquids* **5**, 333–344. Univ. of Missouri-Rolla.

Browand, F. K. & Wiedman, P. D. 1976 *J. Fluid Mech.* **76**, 127.

Brown, G. L. & Roshko, A. 1974 *J. Fluid Mech.* **64**, 775.

Chan, Y. Y. 1974 *Phys. Fluids* **17**, 1667.

Clark, A. R. 1979 Ph.D. thesis, Univ. of Houston.

Crighton, D. G. & Gaster, M. 1976 *J. Fluid Mech.* **77**, 397.

Crow, S. C. & Champagne, F. H. 1971 *J. Fluid Mech.* **48**, 547.

Davies, P. O. A. L. & Baxter, D. R. J. 1978 *Structure and Mechanisms of Turbulence I* (ed. H. Fiedler), Lecture notes in Physics, vol. 75, p. 125. Springer.

FREYMUTH, P. 1966 *J. Fluid Mech.* **25**, 683.

HILL, R. G., JENKINS, R. C. & GILBERT, B. L. 1975 *Grumman Res. Dept. Rep.* RE-508.

HUSSAIN, A. K. M. F. & CLARK, A. R. 1977 *Phys. Fluids* **20**, 1416.

HUSSAIN, A. K. M. F. & CLARK, A. R. 1980 *J. Fluid Mech.* (to appear).

HUSSAIN, A. K. M. F., KLEIS, S. J. & SOKOLOV, M. 1980 *J. Fluid Mech.* **98**, 97.

HUSSAIN, A. K. M. F. & REYNOLDS, W. C. 1970 *J. Fluid Mech.* **41**, 241.

HUSSAIN, A. K. M. F. & ZAMAN, K. B. M. Q. 1975 *Proc. 3rd Interagency Symp. Trans. Noise, Univ. of Utah*, pp. 314–325.

HUSSAIN, A. K. M. F. & ZAMAN, K. B. M. Q. 1978 *J. Fluid Mech.* **87**, 349.

HUSSAIN, A. K. M. F. & ZAMAN, K. B. M. Q. 1980 *J. Fluid Mech.* **101**, 493.

HUSSAIN, A. K. M. F. & ZEDAN, M. F. 1978 *Phys. Fluids* **21**, 1100.

KELLY, R. E. 1967 *J. Fluid Mech.* **27**, 657.

KO, N. W. M. & DAVIES, P. O. A. L. 1971 *J. Fluid Mech.* **50**, 49.

KOVASZNAY, L. S. G. 1978 *Structure and Mechanisms of Turbulence I* (ed. H. Fiedler), Lecture notes in Physics, vol. 75, p. 1. Springer.

LAU, J. C., FISHER, M. J. & FUCHS, H. V. 1972 *J. Sound Vib.* **22**, 379.

MICHALKE, A. 1965*a* *J. Fluid Mech.* **23**, 521.

MICHALKE, A. 1965*b* *J. Fluid Mech.* **22**, 351.

MICHALKE, A. 1972 *Prog. Aero. Sci.* **12**, 213.

MIKSAD, R. W. 1972 *J. Fluid Mech.* **56**, 695.

MOORE, C. J. 1977 *J. Fluid Mech.* **80**, 321.

PETERSEN, R. A. 1978 *J. Fluid Mech.* **89**, 469.

PETERSEN, R. A., KAPLAN, R. E. & LAUFER J. 1974 *N.A.S.A. Contractor Rep.* no. 134733.

PFIZENMAIER, E. 1973 Doktor-Ingenieur thesis, Technischen Universitaet Berlin.

ROCKWELL, D. O. 1972 *J. Appl. Mech.* **39**, 883.

ROSHKO, A. 1976 *A.I.A.A. J.* **10**, 1349.

SAFFMAN, P. G. 1978 *Structure and Mechanisms of Turbulence II* (ed. H. Fiedler), Lectures notes in Physics, vol. 76, p. 273. Springer.

SATO, H. 1960 *J. Fluid Mech.* **7**, 53.

SOKOLOV, M., HUSSAIN, A. K. M. F., KLEIS, S. J. & HUSAIN, Z. D. 1980 *J. Fluid Mech.* **98**, 65.

TOWNSEND, A. A. 1956 *The Structure of Turbulent Shear Flow.* Cambridge University Press. (Reprinted in 1976.)

VLASOV, Y. V. & GINEVSKIY, A. S. 1974 *N.A.S.A.* TTF-15, 721.

WINANT, C. D. & BROWAND, F. K. 1974 *J. Fluid Mech.* **63**, 237.

YULE, A. J. 1978 *J. Fluid Mech.* **89**, 413.

ZAMAN, K. B. M. Q. 1978 Ph.D. thesis, Univ. of Houston.

ZAMAN, K. B. M. Q. & HUSSAIN, A. K. M. F. 1981 *J. Fluid Mech.* (to appear).

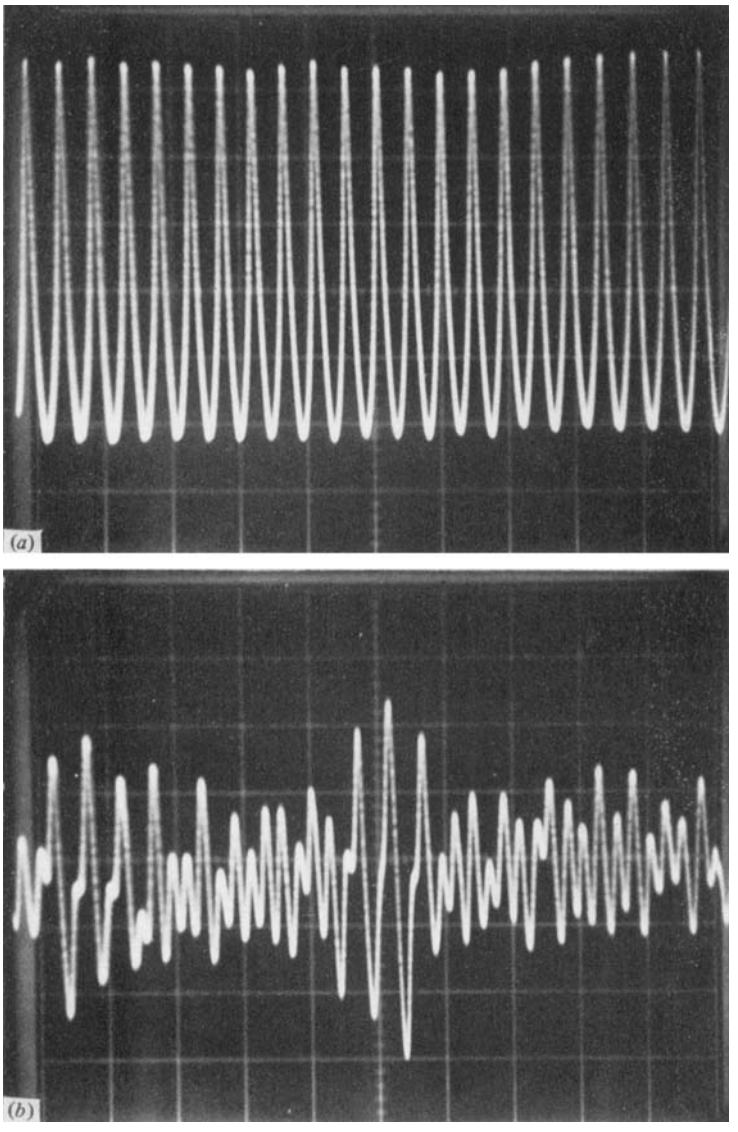

FIGURE 18. Oscilloscope trace of centre-line $\tilde{u}$ signal; $D = 2{\cdot}54$ cm; $x/D = 2$; $f_p = 452$ Hz; $St_D = 0{\cdot}85$; $Re_D = 23000$, with exit boundary layers: (*a*) laminar; (*b*) turbulent. Identical horizontal scales; vertical scale of (*b*) is half that of (*a*).

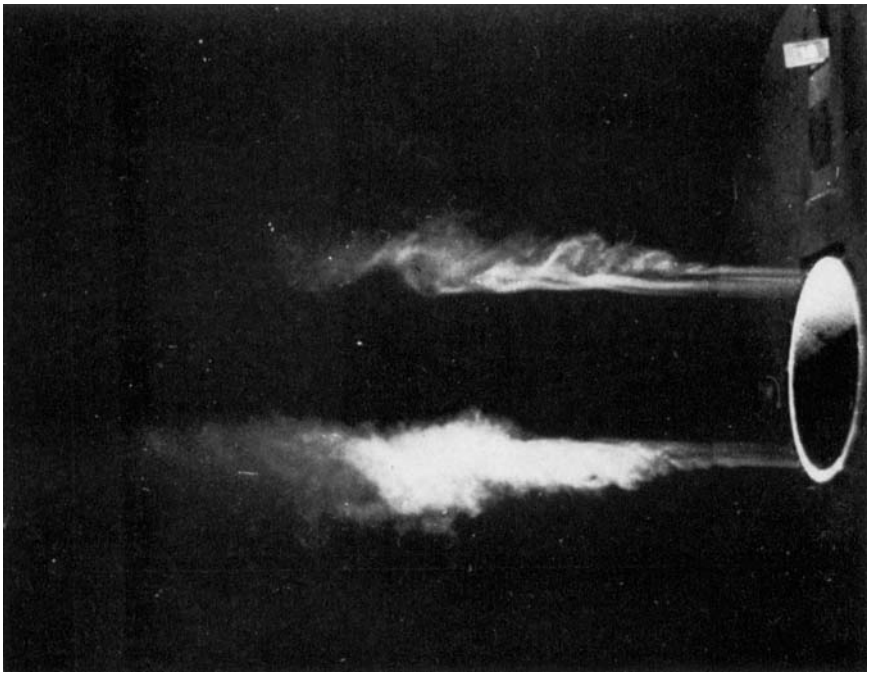

FIGURE 21. Smoke picture of the 7·62 cm unexcited jet at $Re_D = 32000$.

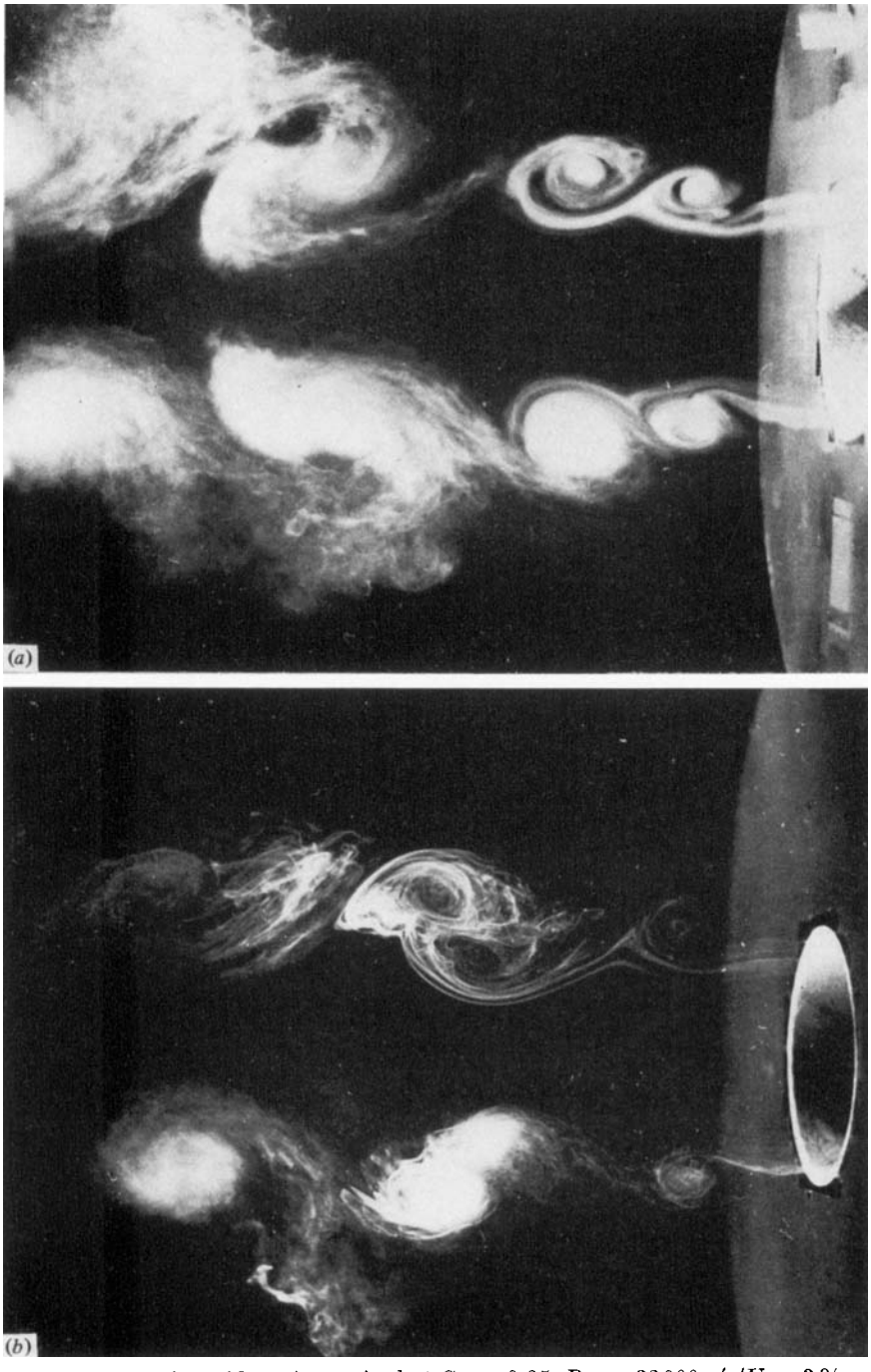

FIGURE 22. The 7·62 cm jet excited at $St_D = 0{\cdot}85$, $Re_D = 32000$ $u'_{ec}/U_e = 3\,\%$. Pictures (*a*)–(*b*) represent two successive phases of the pairing process.

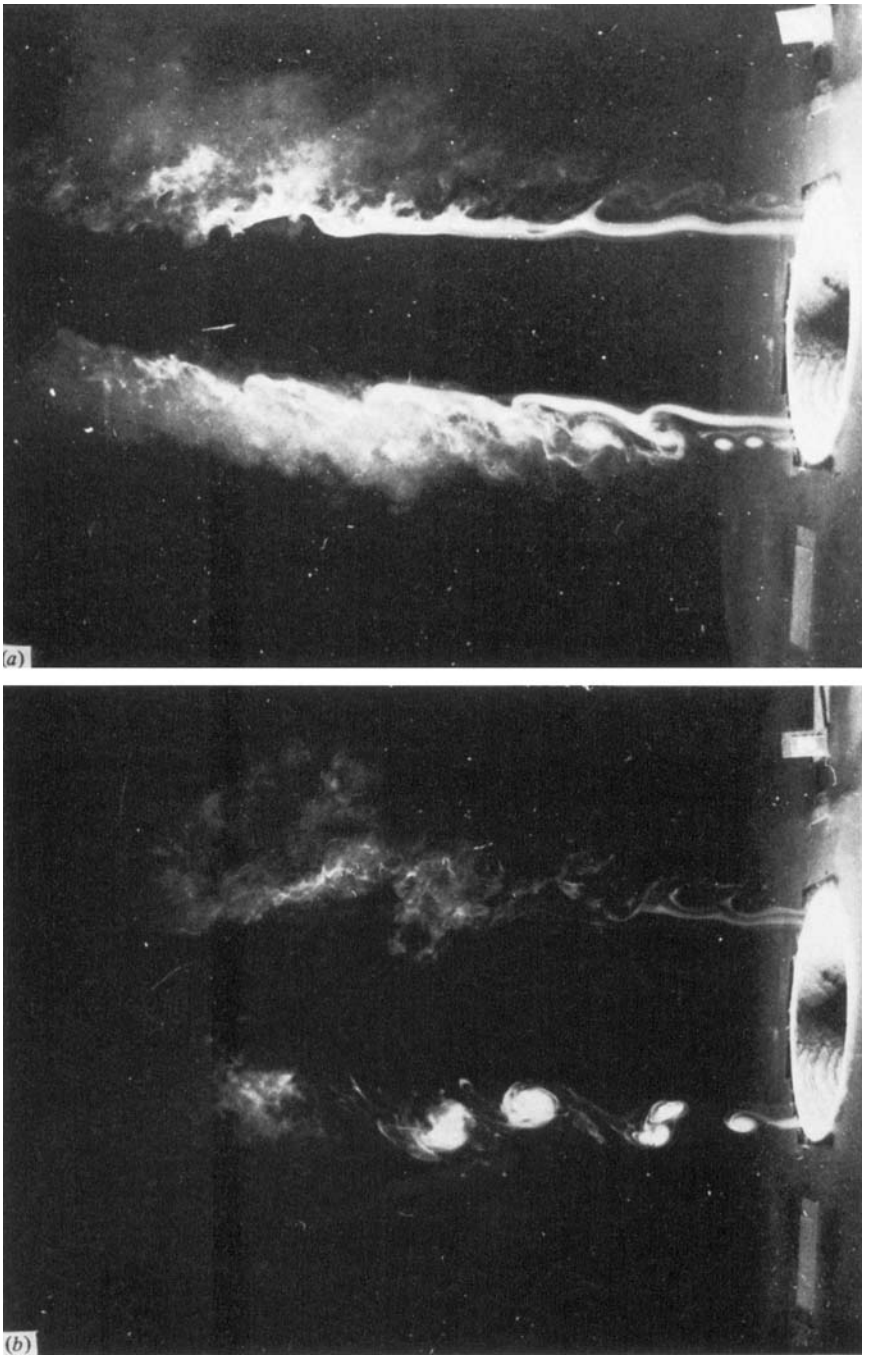

FIGURE 23. The 7·62 cm jet excited at $St_\theta = 0{\cdot}011$, $u'_{ec}/U_e = 1\,\%$.
(*a*) $Re_D = 32\,000$ ($St_D = 3{\cdot}77$); (*b*) $Re_D = 11\,300$ ($St_D = 2{\cdot}41$).

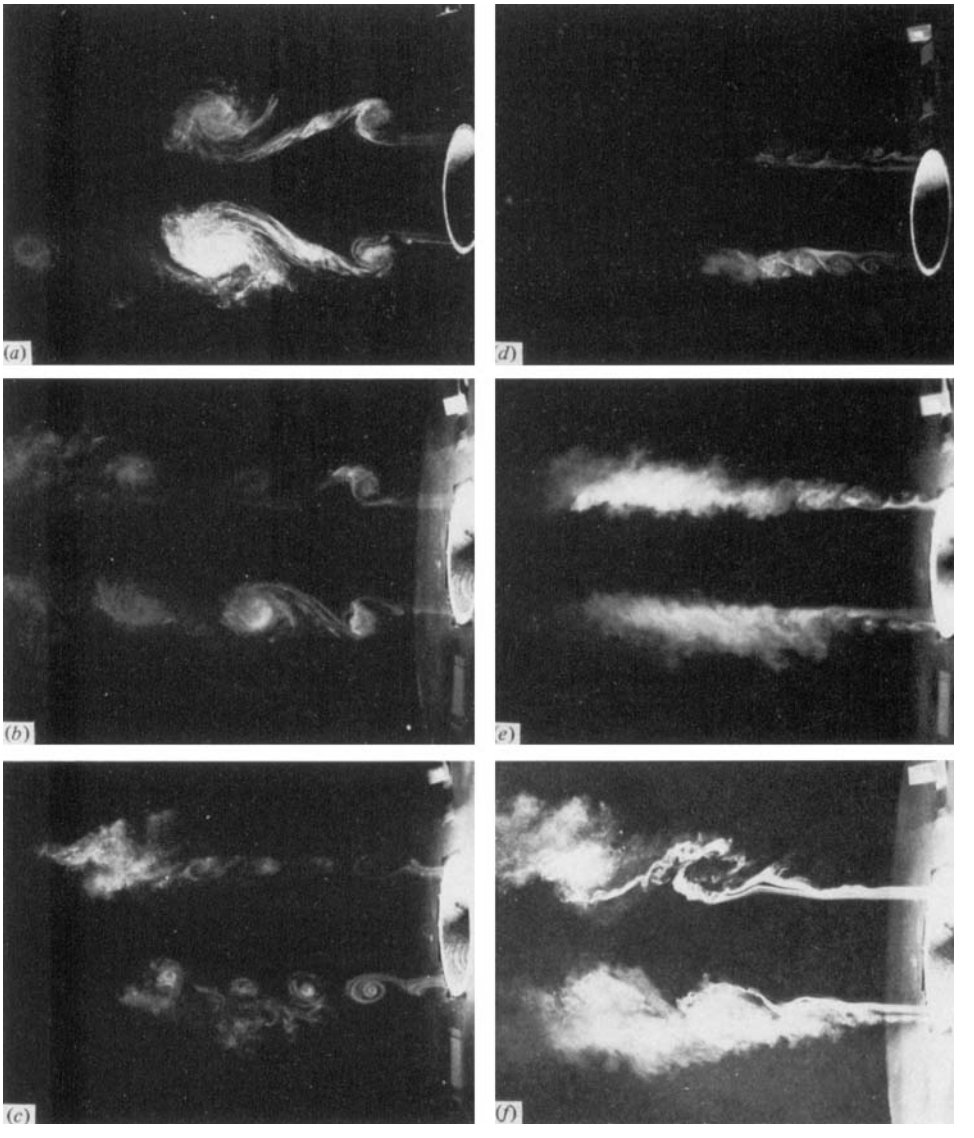

FIGURE 24. The 7·62 cm excited jet. Values of St_D, St_θ and Re_D are: (*a*) 0·425, 0·0011, 42000; (*b*) 0·60, 0·0016, 42000; (*c*) 1·20, 0·0033, 36000; (*d*) 1·60, 0·0041, 43000; (*e*) 3·02, 0·008, 40000; (*f*) 4·69, 0·015, 26000.

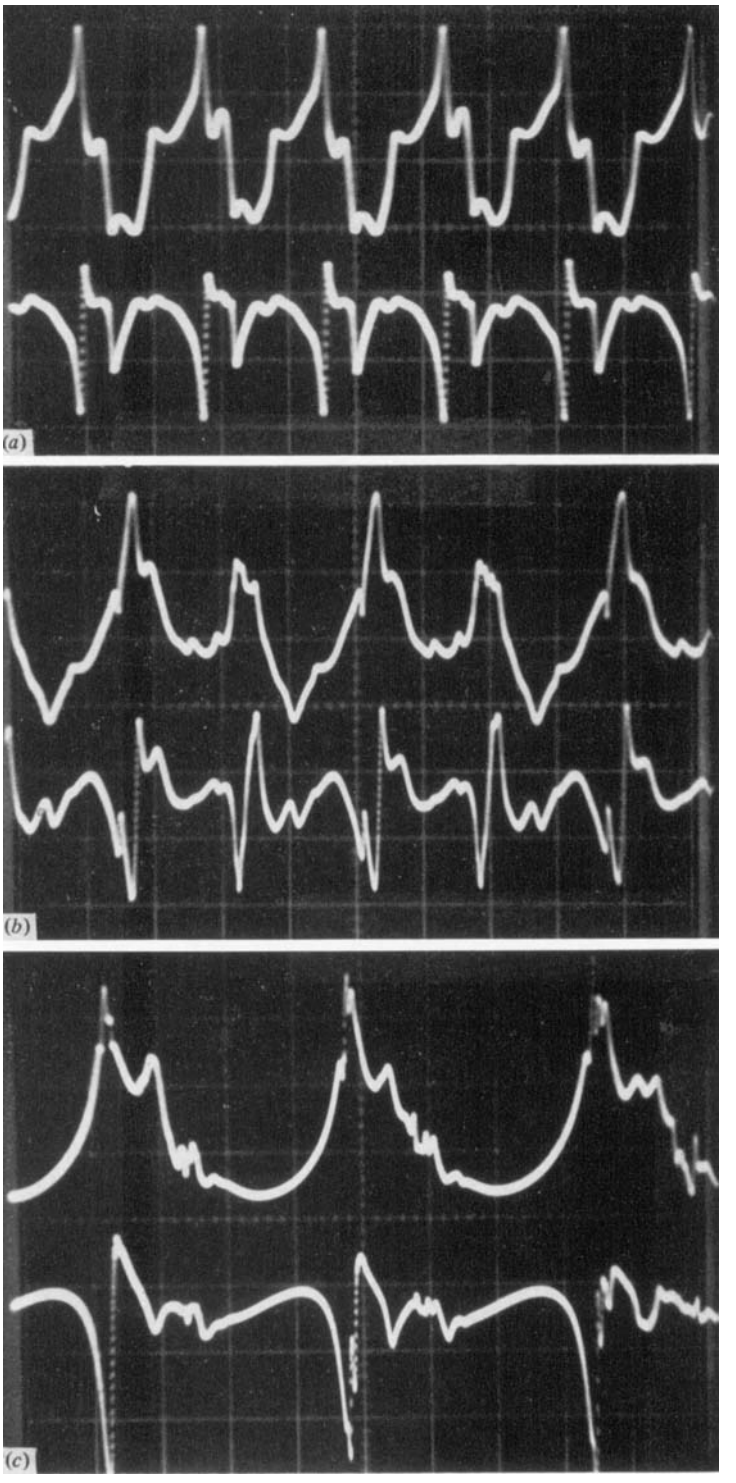

FIGURE 30. Oscilloscope traces of $\tilde{u}$ (upper) and $\widetilde{uv}$ (lower) at the locations of the peak $-\overline{uv}$. $D = 7{\cdot}62$ cm; $St_D = 0{\cdot}85$; $Re_D = 32\,000$; $u'_{ec}/U_e = 3\,\%$. (*a*) $x/D = 0{\cdot}3$; (*b*) $x/D = 0{\cdot}6$; (*c*) $x/D = 1{\cdot}75$.